BIOTIN-CONJUGATED CELLULOSE NANOFIBERS PREPARED VIA CUAAC “CLICK” CHEMISTRY

A Thesis

Presented to the Faculty of the Graduate School

of Cornell University

in Partial Fulfillment of the Requirement for the Degree of

Master of Science

by

Katarina Elise Goodge

May 2020

ABSTRACT

Biotin-cellulose nanofiber membranes were developed for use in diagnostic tools. Cellulose acetate (CA) was electrospun into a nonwoven, nanofibrous membrane that was either directly functionalized with propargyl bromide or was first deacetylated (RC) then substituted with propargyl bromide (alkyne-RC). Fourier-transform infrared spectroscopy (FTIR) and Raman spectroscopy were utilized to relate the alkyne peak height ratios to alkyne substitution. The alkyne substitution reaction was dependent on solvent ratio, time, and temperature with optimal reaction conditions of RC in 80/20 (v/v) isopropanol to water at 50°C for 6 hours. Azide-biotin conjugate was “clicked” onto the alkyne-grafted cellulose nanofiber surface via Copper-catalyzed Alkyne-Azide Cycloaddition (CuAAC). FTIR confirmed successful biotin addition. Scanning Electron Microscopy (SEM) verified the nanofiber morphology at each functionalization step. Energy Dispersive X-ray spectroscopy (EDX) mapped the biotin distribution on the membranes. X-ray Photoelectron Spectroscopy (XPS) quantified the total biotin on the nanofiber surface. The biotin-cellulose nanofiber membranes were used in example assays (HABA colorimetric assay and fluorescently-tagged streptavidin assay) where streptavidin specifically bound to the pendant biotin without the need for a blocking agent. The click reaction was specific to only the alkyne-azide coupling and was dependent on pH, ratio of ascorbic acid to copper sulfate (AA:Cu), and time. Copper (II) reduction to copper (I) was successful without use of the ascorbic acid reducing agent, increasing the viability of the click conjugation method with biomolecules. The surface available biotin was found to be dependent on storage medium and time: biotin was unavailable after 24 hours in water but recovered over a period of months with storage in air.

BIOGRAPHICAL SKETCH

Katarina Goodge was born and raised in Chardon, Ohio. In May of 2014, she graduated from Chardon High School and the following fall entered the department of Chemical and Biomolecular Engineering at The Ohio State University, where she received her Bachelor of Science in Chemical Engineering and minor in Fashion Retail Studies in May 2018.

In August of 2018, Katarina began her Master of Science program in the Fiber Science and Apparel Design department at Cornell University. She has held four summer internships in the commercial R&D sector while working towards her Bachelor and Master's degrees. After completion of her MS degree, Katarina will continue her Ph. D under the advisement of Dr. Margaret Frey.

ACKNOWLEDGEMENTS

The completion of this thesis would not have been possible without the support system surrounding me. First and foremost, I would like to express my gratitude towards my adviser, Dr. Margaret Frey. Her spirit of adventure regarding research and excitement for teaching has been the greatest inspiration. Her kind but persistent guidance has shaped this present work and me as a woman in science. Additional thanks to the merry band of ChemE misfits from the Frey research group.

I also extend appreciation for my minor committee member, Dr. Christopher Alabi, from the Smith School of Chemical and Biomolecular Engineering. His insight pushed this project to new depths.

I am grateful for access to the equipment across the Cornell campus and the amazing assistance and training from facility managers and staff. This work made use of the Cornell Center for Materials Research Shared Facilities which are supported through the NSF MRSEC program (DMR-1719875). Imaging data was acquired through the Cornell University Biotechnology Resource Center, with NIH 1S10RR025502 funding for the shared Zeiss LSM 710 Confocal Microscope.

Lastly, I express my undying gratitude towards my family and friends who have helped me traverse the turbulence and ardor of personal growth.

TABLE OF CONTENTS

LIST OF FIGURES

LIST OF TABLES

1. INTRODUCTION

Both communicable (eg. tuberculosis) and noncommunicable diseases (eg. diabetes and cancer) continue to make World Health Organization's Top 10 Causes of Death list.[1] Early and accurate detection is vital as it reduces the chances of death or the severity of the disease prognosis. Current clinical diagnostics rely on assays, imaging, and tissue biopsy, with limited access for impoverished areas of the world.[2] These technologies are typically expensive, time consuming, require trained technicians, and often are not sensitive or specific enough to be conclusive.

Current biosensor research tackles performance issues by immobilizing probes on planar surfaces in point-of-care devices. However, the largest drawback is that the poor surface area limits the attachment of probes, directly correlating to lower sensitivity and higher response time.[2] Instead, 3D structures are being explored for their high surface-area-to-volume ratio, enhanced roughness, and porosity. Increased reproducibility is gained from the consequent higher probe loading. Fabrication methods include photolithography, metal etching, and layer-by-layer growth of nanotubes/particles, but these are expensive, time consuming, and process-intensive. Furthermore, the probe immobilization techniques have added drawbacks such as probe leaching, deactivation of probe during immobilization, low loading capacity, and poor shelf life.[3,4,5,6]

Nanofibers are an attractive option due to their ease of formation, high surface area to volume ratio, and range of potential functionalization. This high ratio is crucial in extending the sensitivity of the resulting assay. In this study, cellulose nanofibers were spun via electrospinning, and biotin conjugates were immobilized via click chemistry onto the nanofiber surface within the nonwoven membrane. This biotin-cellulose fibrous

membrane was used to specifically and rapidly detect streptavidin present in the fluid sample based on the biotin-streptavidin binding affinity. The biotin yield as a function of intermediate functionalization and click reaction conditions was characterized. The biotin-streptavidin was used as the affinity model to represent future use of the antibody-antigen model in a nonwoven diagnostic device.

2. PROJECT BACKGROUND

2.1. Electrospinning

Out of the multitude of processing techniques to produce nanofibers, including drawing; template synthesis; phase separation; self-assembly; and electrospinning; electrospinning is the only process that has successfully fabricated nanofiber membranes on an industrial scale.[7] Multi-jet, needle-free spinnerets and roll-to-roll collectors such as Nanospider™, Inovenso, and Bioinicia mitigate the lab-scale drawbacks of low throughput, and adaptable configurations of the equipment make electrospinning an attractive option for a wide range of applications. Electrospinning was patented by Formhals in 1934 and boasts a simple, cost-effective laboratory setup to produce long, filament fibers.[7] Although the setup is simple, the science behind it is much more complex.

Electrospinning can generate fibers over the range of 3 nm to >1 μm, classifying them in the realm of nanofibers and ultrafine fibers. While the technical definition for “nano” constitutes objects with at least one dimension that is 100nm or less, dimensions in the sub-micron range also loosely fall within the category of nanotechnology.[7] Here, nanofibers take on the looser definition of diameters in the nanometer to submicron range that will be used for the remainder of this thesis.

The advantage of nanofibers versus other structures originates in the change of scale. As the diameter of the fiber decreases from conventional fibers (microns) to submicron to nanometer, the surface area to volume ratio increases. The higher ratio of surface to bulk allows for higher number of functional groups at the surface. This translates to higher efficiency of the intended end-use as well as more flexibility in modifying the surface functionalities. The properties of nanofibers versus conventional fibers are well studied, and cellulose fibers will be specifically discussed in more detail in section 2.2 and 2.3.

Electrospinning has a multitude of advantages over alternative methods to form nanofibers. The basic laboratory setup is modular and easily adaptable. Components are easily manipulated to tailor the resulting properties of the individual fibers and overall nonwoven structures. A range of polymers can be used in their melt, solution, or other form. Even polymers that do not form fibers from other methods can be electrospun into nanofibers. A useful overview of the fundamentals of nanofiber formation via electrospinning has been published.[7]

The components of the electrospinning process include a spinneret (syringe with needle), a high voltage source, and a grounded collector. A schematic of the process is shown in Figure 2.1. Applied voltage supplies electrostatic forces to the solution at the spinneret tip. Once these forces overcome the surface tension of the solution, a Taylor cone is formed.[7] The charged fluid jet travels towards the grounded collector due to the difference in potential.[7] Repulsive forces between charges on the electrospinning jet cause a bending instability and stretching of the solution.[7] The solvent evaporates as a single fiber, which subsequently is attenuated in the air gap and collected on the grounded

collector. Over time, a nonwoven fabric is formed by the overlapping fibers, with a large interconnected porous network.

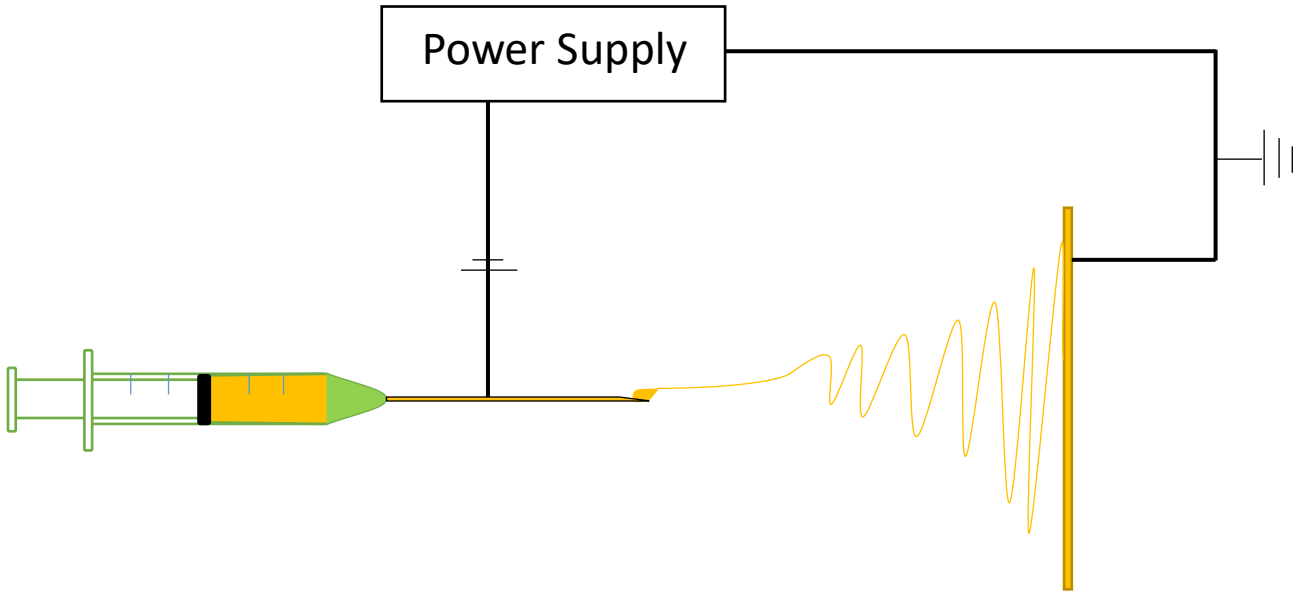

Figure 2.1: Electrospinning process schematic

The fiber formation process and resulting fiber properties are dependent on solution parameters, spinning conditions, and ambient conditions. Solution parameters include solution viscosity, solvent system affinity with polymer, solvent volatility, and solution conductivity. Spinning condition considerations include solution flow rate, applied voltage, distance to collector, radius of spinneret, and choice of collector. Ambient conditions consist of relative humidity and temperature. These variables are discussed in-depth in the review.[7]

Although nanofibrous membranes are excellent for basic applications, they require chemical or physical modification in order to create active sites within the resulting membrane.[8] These modifications can take place either pre- or post-spinning and mostly affect the bulk and surface properties, respectively.[8] In the interest of protein

immobilization within nanofiber membranes, pre-spinning modifications would not be particularly strategic since functionalization would occur both in the bulk and on the surface of the fibers, and the efficiency would be hindered by the inaccessibility of the functional groups within the bulk.[8] These difficulties are made simpler by instead modifying the polymers after they have been electrospun into nanofibers.

2.2. Cellulose Acetate

Cellulose acetate (CA) is a low-cost polymer from a renewable source with suitable spinnability and ability to readily functionalize with various chemistries. The acetyl groups can be modified directly or deacetylated to regenerate the hydroxyl groups. CA was first made by Paul Schützenberger in 1865.[9] It is the acetate ester of cellulose with a typical degree of substitution between 1 and 3, shown in Figure 2.2. The degree of substitution is calculated based on the number of functional groups that replace the hydroxyl groups in the anhydroglucose unit (AGU).

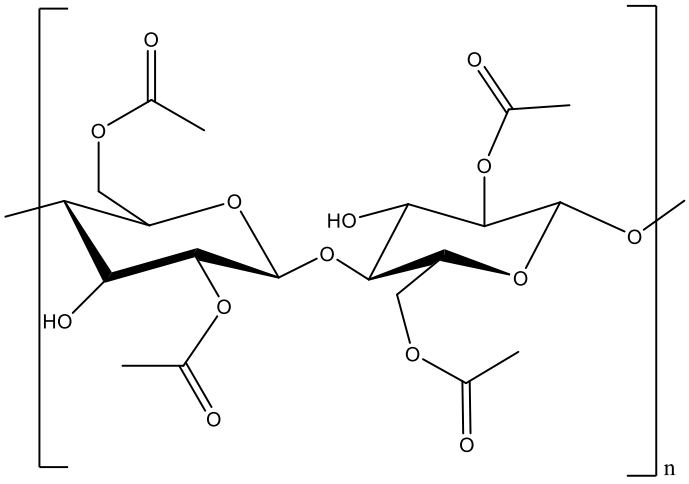

Figure 2.2: Chemical structure of CA repeat unit

Commercially it is known for its low absorption characteristics (high throughput) and thermal stability with high flow rate. CA is commonly used in semi-permeable membranes such as dialysis, ultrafiltration, and RO, as well as biomedical applications.[7]

Cellulose is not readily soluble in solvents suitable for electrospinning. Many researchers, however, have reported successful electrospinning of CA.[10] When choosing the solvent system for CA, the solubility, volatility, and conductivity were considered. In past studies, CA has been spun out of DMAc, acetone, acetic acid, DCM, and combinations thereof.[9,11,12,13,14] CA was observed to dry on the tip of the needle during spinning due to the high volatility of these solvents. Co-solvents (ie. solvents with higher boiling points such as methanol and water) were added to decrease the evaporation rate allowing enough time for fibers to solidify in the air gap without clogging the spinneret tip.[11] Both Hildebrand and Hansen solubility parameters can be used to predict suitable solvent combinations. Since CA has strong hydrogen bonding, the Hildebrand parameters can only give a rough estimate for solubility of CA based on nonpolar polymer interactions. Therefore, Hansen solubility parameters, which include polar interactions, were calculated for the DCM/methanol system and acetone/acetic acid/ water system. Equations 2.1, 2.2, 2.3 are used to calculate the Hansen solubility parameters and RED ratio:

$$\delta_T^2 = \delta_D^2 + \delta_P^2 + \delta_H^2 \tag{2.1}$$

$$(Ra)^2 = 4(\delta_{D2} - \delta_{D1})^2 + (\delta_{P2} - \delta_{P1})^2 + (\delta_{H2} - \delta_{H1})^2 \tag{2.2}$$

$$RED = \frac{Ra}{Ro} \tag{2.3}$$

where δ is the solubility parameter for total (Hildebrand) (T), dispersion (D), polar (P), and hydrogen bonding (H) cohesion, Ra is the distance in Hansen space, Ro is the radius of interaction sphere in Hansen space, and RED is the relative energy difference.[15]

Table 2.1 lists the parameters for each of the solvents. When RED <1, the solvent is categorized as good for the polymer. When RED approaches 1, the solubility reaches a boundary condition. When RED >> 1, the solvent has low affinity for the polymer.[15]

Table 2.1: Hansen Solubility Parameters and RED ratios for solvent candidates

(Calculated using 13, 15, 16)

Solvent	Hansen Solubility Parameter ($MPa^{1/2}$)[16]				Ra	Ro	RED	Good solvent?
	d_t	d_d	d_p	d_h				
DCM	20.31	18.22	6.34	6.14	8.33	-	0.671559	Yes
methanol	29.20	15.17	12.27	22.29	12.33922	-	0.995098	Boundary
acetone	19.98	15.50	10.43	6.95	5.45	-	0.439708	Yes
acetic acid	21.47	14.52	7.98	13.50	2.66	-	0.214753	Yes
water	48.06	12.27	31.29	34.15	33.82488	-	2.727813	No
CA	19.89	14.9	7.1	11.1	-	12.4 [13]	-	-

Water is miscible with acetone and a nonsolvent for CA, but it can still be used to decrease the volatility of the solution.[11] Methanol is considered on the boundary, but in low percentages won't disrupt the solubility of CA in the main solvent while decreasing the evaporation rate of the solution. The Hansen solubility parameters indicate that these solvents are a good starting point, but using mixed solvents requires empirical testing to determine the correct ratio.

Additional consideration is given to the conductivity of the solvents. The conductivity of DCM and methanol is 0.034 mS/m and 0.1207 mS/m, respectively. The dielectric constants of DCM and methanol are 8.93 and 32.6, respectively. The conductivity of acetone and distilled water is 0.0202 mS/m and 0.447 mS/m, respectively. The dielectric

constants of acetone, acetic acid, and water are 20.7, 6.15, 80.2, respectively.[9] Higher conductivity aids in the stretching of the jet; increasing the jet whipping instability and the jet path, therefore decreasing the fiber diameter and produce smoother fibers.[7] Although both solvent systems have been reported to successfully produce fibers, DCM and methanol was ultimately chosen as the solvent system. Tungpara et al. concluded that the CA fibers were systematically larger from DCM/methanol solution than acetone/DMAc solution despite the lower shear viscosity and conductivity. Elongational viscosity was not measured, which could better describe the divergence of the results. The optimal electrospinning conditions for CA in DCM/methanol was 8-12% (w/v) CA in 4:1 (v/v) DCM/methanol with 15 kV applied voltage and 15 cm tip-to-collector distance. Relative humidity and feed rate were not specified.[9]

CA is an insulator and static charges will accumulate during electrospinning. The charges on the fibers cause the new layers to repel from the layers that have already been deposited onto to the collector. Liu and Hsieh found that this challenge can be mitigated with the collector type. Using a grounded copper plate wrapped in aluminum foil is the best choice of collector to dissipate the charges and increase the packing density.[12]

De Vrieze et al. studied the effect of ambient temperature and relative humidity on the fiber formation of CA. They noted that the “evaporation rate for a pure liquid from a free surface is proportional to the difference of the saturated vapour pressure and the vapour pressure in the surrounding air of the solvent.” Even with a system that does not contain water as a solvent, the fiber formation was found to be dependent on the relative humidity. Additionally, the evaporation rate of ethanol was found to be independent of RH. They hypothesized that it was water acting as a nonsolvent that caused the RH dependency.

During the jet acceleration through the air gap, the CA absorbs the ambient water vapor and causes the CA to precipitate. Increasing the RH allows for more water to come in contact with the jet, which causes the fibers to form faster, inhibit the stretching of the jet, and result in larger fibers.[14]

2.3. Regenerated Cellulose

Once the CA is electrospun into nanofibers, the surface can be directly functionalized, or the acetyl groups can be removed before modifying the surface chemistry. Deacetylating the CA regenerates the hydroxyl groups of cellulose II allomorph, as shown in Figure 2.3, into regenerated cellulose (RC).

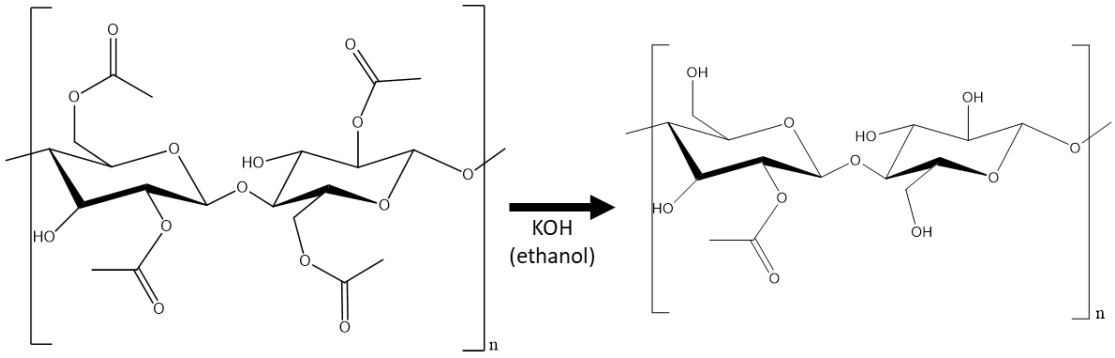

Figure 2.3: Chemical reaction for deacetylating CA to RC

The advantage of regenerating the cellulose nanofibers is the change in chemical resistance of cellulose versus CA in most organic solvents and aqueous solution in pH range 3-12. This is relevant for both the alkyne substitution and click reaction steps. The change in reactivity of the carbon-6 from acetyl group (acetic acid pKa = 4.75) to hydroxyl group (pKa ~ 12.2) accounts for the higher stability of cellulose in alkaline

solutions versus CA.[11] In addition to the advantage of cellulose nanofibers over CA nanofibers, cellulose nanofibers also have special properties compared to conventional, native cellulose. The nanoscale versus microscale of the respective fiber increases the surface availability of the hydroxyl groups as well as increases the water and chemical absorbency due to increase in capillary action of the smaller pore sizes.[11,12] The combination of higher surface area and lower crystallinity of cellulose nanofibers compared to conventional cellulose fibers is highly desirable for surface-supported reactions due to the accessibility of the hydroxyl groups.

The deacetylation reaction can be carried out in alkaline aqueous or alcoholic solution. Liu and Hsieh found that the hydroxide in ethanol solution was more effective at homogeneously removing the acetyl groups throughout the entire volume of fiber whereas the aqueous solution targeted the surface acetyl groups without penetrating the fiber core. Both methods maintained their fiber morphology, but the reaction was faster and more efficient in ethanol.[12] For this study, the deacetylation must be complete so that residual acetyl groups do not compete with the alkyne substitution reaction. Therefore, the alcoholic deacetylation was chosen.

2.4. Biotin Immobilization: Heterogeneous Chemoselective Ligation

The simplest technique for immobilizing molecules onto substrate surfaces is physical techniques such as adsorption and entrapment. These are not sufficient methods for applications that have a two-fold challenge: the immobilized biomolecules must maintain their functionality while also remaining on the substrate surface without leaching during

washing or storage.[17] These two challenges can be overcome by permanently attaching the biomolecules to the substrate with covalent linkages.

Post-spinning modification functionalizes the surface of the nanofibers, and various chemical methods can be employed. Mahmoudifard et al. used EDC/NHS coupling agents to immobilize anti-staphylococcus enterotoxin B (anti-SEB) on polyethersulfone (PES) for use in microfluidic diagnostic devices.[3] Rodriguez-deLuna et al. crosslinked horseradish peroxidase enzyme onto polyvinyl alcohol (PVA) nanofibers by exposing them to glutaraldehyde (GA) vapor.[4] Afshari et al. tested various plasmas to immobilize glucose oxidase onto PVA-malonic acid fibers.[5] Non-selective attachment can be achieved through potentially simpler reaction conditions or fewer steps, depending on which substrate and which biomolecule is used. Widely used techniques such as EDC/NHS coupling of an amine group on the protein and a carboxylic acid on the substrate or reductive amidation of an amine and aldehyde require that the amine group on the protein not be involved in the bioactivity of the protein. This limits the available biomolecules that can be immobilized, or it puts the biomolecule at risk of losing its bioactivity once immobilized. The chance of biomolecules losing their bioactivity depends on which site on the biomolecule participated in the attachment to the nanofiber and whether it was an active site that determines the bioactivity of the overall biomolecule. If deactivated proteins remain on the nanofiber surface, they can cause problems down the road with nonspecific adsorption of non-target species in the detection sample. These potentially cannot be blocked using a generic blocking agent since the functional groups on the protein are not the same functional groups on the substrate and would require additional blocking treatment to ensure that the inactive proteins are not nonspecifically

adsorbing molecules that might interact with their multitude of available amino acids. In addition, molecules in the sample can possibly get physically entangled by the increased tortuosity of the porous nanofibers that have a high degree of inactive proteins attached. This can also affect the sensitivity of the resulting biosensor since the biomolecule loading onto the fiber is limited by the amount of inactive, nonspecific biomolecule loading that occurs. Most simply, nonspecific coupling is not a cost-effective option due to the expensive proteins that must be sacrificed to achieve the desired degree of substitution of active proteins. While the coupling chemistries mentioned above have been proven to have varying degrees of success in short-term stability, reusability, and bioactivity, these methods are susceptible to hydrolysis and degradation with long-term storage.[18]

Previously, biotinylated polymers were electrospun, and then streptavidin was specifically bound to the biotin on the fiber surface. Biotinylated biomolecules could further bind to the streptavidin to effectively immobilize the desired biomolecule onto the fiber surface.[19] Although this process is scalable, it requires a multitude of steps with expensive reagents. In addition, even though the biotin-streptavidin binding is one of the strongest non-covalent bonds in nature, the biotin can still leach from the fibers when placed in water, even when biotin is covalently attached to the fiber.[6,20] Shephard et al. showed that with biotin covalently-linked poly(lactic acid) (PLA) fibers, biotin leaches from the fiber over time in an aqueous environment and that the time-dependence of the system's properties reaches an equilibrium.[6] As most applications of the functionalized nanofibers will be filtration, microanalytical devices, catalysts, etc., this water instability is unfavorable.

In this work, a relatively new post-electrospinning modification strategy, click chemistry, is employed. Click chemistry is a class of specific reactions characterized by relatively

fast, catalyzed reactions, high efficiency, high selectivity, and stable reactants that was originally named by Karl Barry Sharpless in 1998.[21] A key advantage of click reactions is that they are bio-orthogonal, and therefore, proteins can participate in the reactions while retaining their bioactivity.[21] The covalent bonding of the protein directly to the nanofiber membrane lends to a higher degree of permanence of immobilization and therefore, longer stability. The number of attachment steps to achieve biomolecule immobilization is reduced, and the triazole ring formed is a more stable covalent attachment method.[21] Biotin is used here as a model biomolecule to be able to demonstrate the click potential, but the future target biomolecules are intended to be directly immobilized to the fiber by having an alkyne or azide moiety.

The specific click reaction used in this work, copper-catalyzed azide-alkyne cycloaddition (CuaAAC), provides the advantage of having site-specific attachment of the terminal alkyne and azide-bearing molecules. This is important for biomolecules because their bioactivity can be lost if nonspecific attachments occur at sites that, upon attachment to the external substrate, cause loss of the molecule's biomolecular structure. For click chemistry, there is no worry about inactivated biomolecules because the bioactivity is preserved with the bio-orthogonal click reaction. In addition, the alkyne attachment reaction to the nanofiber and the click reaction between the alkyne and azide are both achieved under mild conditions, with the latter performed in an aqueous solution at room temperature. The copper-catalyzed reaction is irreversible and highly selective to only couple azides and alkynes to form a triazole ring, which is similar to the peptide bond found in natural biomolecules. Topological and electronic similarities of the triazole ring to the peptide bond provide an additional advantage to using click chemistry as certain

biological activity can be mimicked from the peptide bond without having to worry about the susceptibility of hydrolytic cleaving.[22] “Even under relatively extreme conditions used in some biological operations involving the addition of denaturants, detergents, chaotropic agents, organic solvents, or acidic or basic conditions, the triazole ring will survive and remain intact.”[18]

The proposed reaction scheme, shown in Figure 2.4, involves two atoms of copper per triazole ring formation. Sharpless originally proposed a single copper atom mechanism, but recent investigations have proven that the two-atom mechanism is more probable. The first copper atom coordinates with the alkyne group while the second copper atom removes the acidic hydrogen to form the acetylide. The electron-rich alkyne forms a covalent bond with the terminal nitrogen of the azide group, and the coordinated coppers anchor the tertiary nitrogen to form the new heterocycle. The reaction is complete when the first copper disassociates, and the hydrogen replaces the copper to fully regenerate the catalyst.

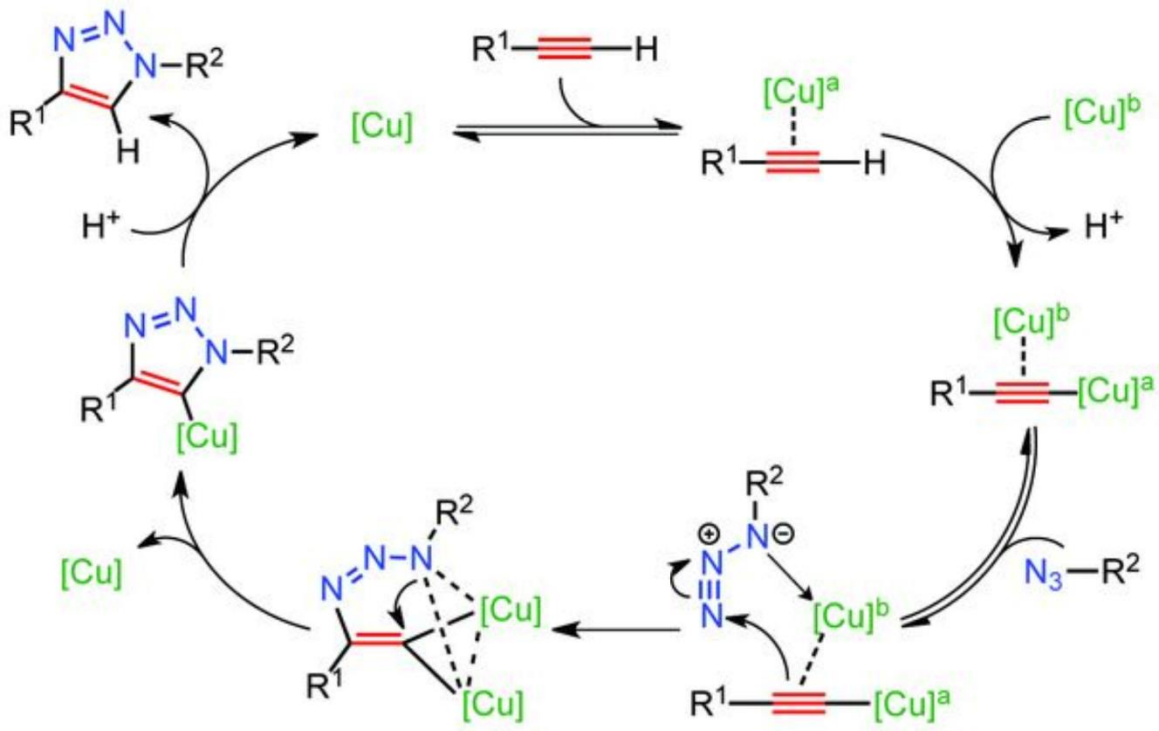

Figure 2.4: The click mechanism involves two copper atoms associating with the alkyne to aid in the cycloaddition of the azide to form the triazole ring[23] (1)

Copper I can be obtained by oxidizing solid copper pieces, using copper I salts directly, or reducing copper II salts. Here, copper sulfate and ascorbic acid were chosen as copper source and reducing agent, respectively, as they are both readily available and easily reduce copper II to I and oxidize ascorbate to dehydroascorbate. Typical click reactions are carried out with 0.25-2 mol% of copper catalyst, but most click reactions are homogeneous and the copper is free to associate and disassociate with the click reagents easily.[18] Clicking onto the nanofibers is a heterogeneous process and requires both the reagents and catalyst to traverse the tortuosity of the porous membrane before reaching

[1] From Worrell, B. T., Malik, J. A., & Fokin, V. V. (2013). Direct Evidence of a Dinuclear Copper Intermediate in Cu(I)-Catalyzed Azide-Alkyne Cycloadditions. Science, 340(6131), 457–460. https://doi.org/10.1126/science.1229506. Reprinted with permission from AAAS.

the reaction site. This requires a higher level of catalyst as well as potentially a higher ratio of reducing agent.

Although click chemistry's high selectivity and bio-orthogonality are the main benefits, these characteristics are possible because both alkyne and azide groups do not generally occur in biological systems. This is advantageous for site-specific attachment because only the azide groups or alkyne groups that were specifically intended to attach will participate in the click reaction. However, that also means that the target biomolecules must synthetically obtain an azide or alkyne group without disturbing its bioactivity. While the altering of the biomolecule is out of the scope of this project, it is still important to consider the feasibility of designing such molecules because it directly impacts the practicality of the technology that will result from this project. Two routes have been taken so far in obtaining clickable biomolecules: specific and nonspecific attachment. An example of nonspecific attachment is the nucleophilic substitution of the azide group with a variety of possible substituents within the biomolecule. Since the substitution is not site-specific, the nonspecific attachment of the azide to the protein negates the purpose of employing the click chemistry strategy. The study does not determine the location and degree of azidation; it cites the low concentration of azide groups on the protein as the reason for not directly characterizing the azidated proteins. While it does go on to prove that the clicked antigens that did maintain their bioactivity were successful in specifically binding the corresponding antibodies, the paper did not address the nonspecific azide attachment to the antigen and its effect on the activity of the protein.[20] Using specific attachment methods quickly increases the complexity of the functionalization process because most biomolecules require careful engineering to get azide or alkyne moieties

artificially introduced. Protein engineering is a complex design process that in and of itself is a huge undertaking. As the strengths of click chemistry are increasingly realized by the wider scientific community, the focus on protein engineering of the clickable proteins can also be increased. This would increase the feasibility of scaling up the click chemistry process into practicable applications.

Click chemistry is not the only method being explored to specifically attach biomolecules to solid substrates. However, using other specific attachment methods require intensive protein engineering. Even though the sortase direct ligation method described by Chan et. al. can attach a wider range of biomolecules to a solid substrate, it requires biomolecular generation of the sortase, which is a complex biomolecular process by itself and is also limited to small-scale production presently.[17]

2.5. Summary of Reaction Scheme

Much of the literature consists of well-established click reactions with small molecules and homogeneous reaction conditions, but heterogeneous clicking onto fibers remains relatively new. Further, the interactive effects of the nanofiber membrane and click reagents are not well studied. Cellulose was chosen as it has familiar textile chemistry to attach the first click reagent (alkyne) onto the fiber. The alkyne group can be attached either directly to CA with sodium hydride as base or, after regeneration of cellulose, with sodium hydroxide as base.[24,25] Propargyl bromide and sodium hydroxide were chosen as the alkyne source and base, respectively, in the Williamson Ether Synthesis (Figure 2.5). The hydroxyl group on the RC is deprotonated by the hydroxide anion and undergoes a

nucleophilic substitution with the propargyl bromide. The alkyne attachment was studied with cellulose pulp by Mangiante et al. and formed the basis of reaction conditions for this study.[25] The overall reaction scheme is shown below in Figure 2.5.

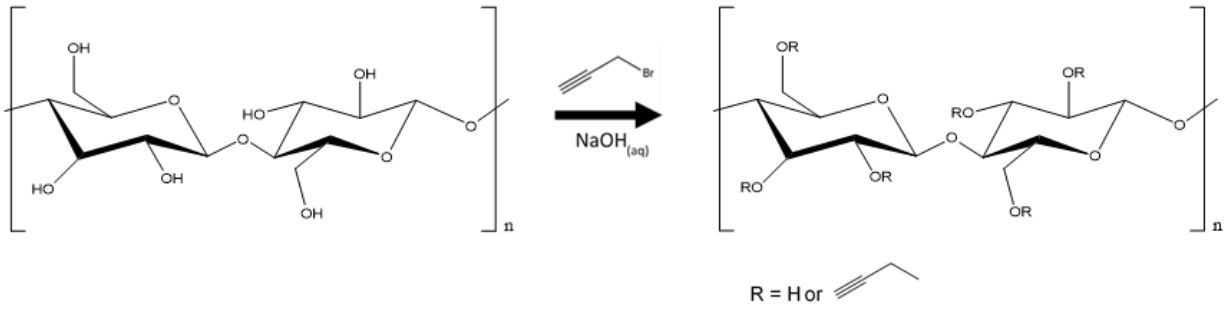

Figure 2.5: Williamson Ether Synthesis of alkyne substitution onto RC

The specific azide-biotin conjugate chosen is commercially available and contains PEG spacers. PEG is hydrophilic and aids in the dissolution of the biotin conjugate in the aqueous click reaction solution as well as increases the biotin conjugate's affinity towards the hydrophilic cellulose. PEG spacers have been shown to enhance "water solubility, increase the hydrodynamic volume of a bioconjugate, extend stability and half-life, and reduce immunogenicity and toxicity of drugs in vivo".[26,27] The presence of PEG groups decreases "nonspecific binding to other biomolecules, thus improving signal-to-noise ratios in assays and potentially enhancing detection sensitivity." [18] The conjugation of the biotin to the cellulose fibers was performed via the CuAAC click reaction (Figure 2.6) with copper sulfate and ascorbic acid as catalyst and reducing agent, respectively.

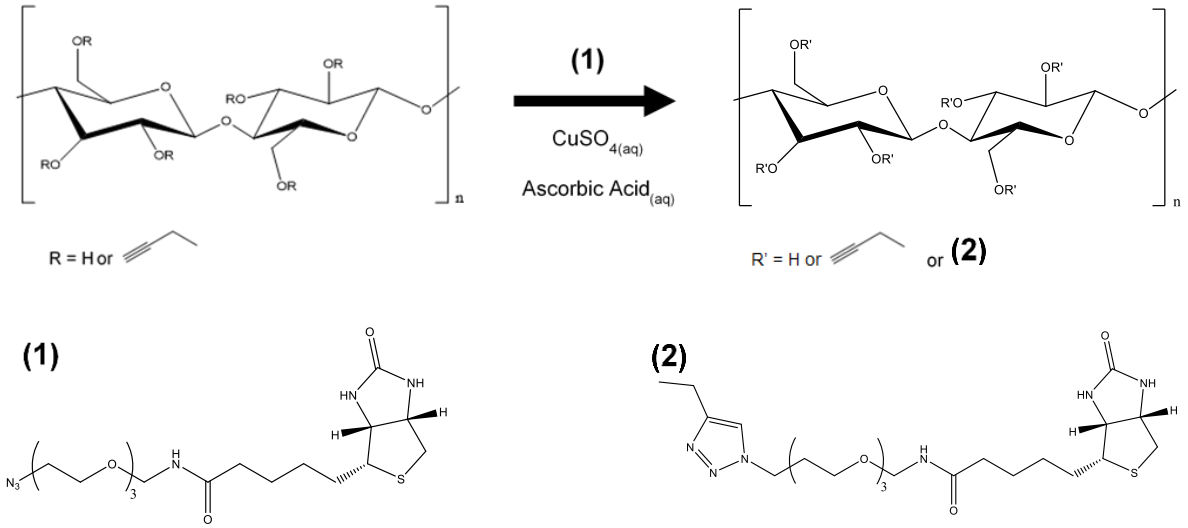

Figure 2.6: CuAAC Click reaction between azide-biotin conjugate (1) and alkyne-RC to form biotin-RC

2.6. End Use: Immobilization of Proteins for Biological Sensing

By covalently bonding biorecognition molecules to nanofibrous membrane, these membranes can then be specialized so that specific antibodies are bonded to the surface of the nanofibers and used as a cheaper, portable diagnostic tool. The nanofiber membrane would act as a handleable physical substrate for the antibodies and assist in the adsorption process. Antigens present in the fluid passing along the membrane would specifically attach to the antibodies. The change in available adsorption sites would translate to whether the antigens are present in the sample or not and could provide an almost immediate result. Further design of the diagnostic device will involve multilayer, sandwich assays and/or multiplexing with multiple target molecules.

It is important to note that while the goal of this study is to use click chemistry to immobilize biomolecules onto nanofibers, this technique also has broader impact. The azide and alkyne graft-to-nanofiber method can be implemented for any application looking to use click chemistry to tailor the nanofiber surface for the desired applications, whether it be biologically related like enzyme catalysis or completely abiotic.

3. MATERIALS AND METHODS

3.1. Materials

Cellulose Acetate (Mn = 30,000, Acetyl content = 39.8%) was purchased from Sigma-Aldrich. Dichloromethane (DCM) (Fisher Chemical), Isopropanol (IPA) (Fisher Chemical), Methanol (Fisher Chemical), Ethanol (Koptec), Potassium Hydroxide (KOH) (Mallinckrodt AR), Sodium Hydroxide (NaOH) (Macron Chemicals), Propargyl Bromide (PBr) (Sigma-Aldrich), L-Ascorbic Acid (Sigma-Aldrich), Copper (II) Sulfate Anhydrous (Sigma-Aldrich), Azide-PEG3-biotin conjugate (Sigma-Aldrich), Streptavidin-FITC from Streptomyces avidinii (Millipore Sigma), and Pierce™ Biotin Quantification Kit (Thermo Scientific) were used without further purification.

3.2. Methods

3.2.1. Electrospinning

Cellulose Acetate (CA) electrospinning solution was prepared at 12% (w/v) polymer concentration in 4/1 (v/v) DCM/methanol solvent mixture. The solution was added to a 5 ml BD plastic syringe (ID = 11.989mm) with BD PrecisionGlide needle (21G, 50mm

length). The syringe was secured horizontally onto a syringe pump (model, supplier). The electrode from the high-voltage power supply (model, supplier) was connected to the needle, and the grounded electrode was connected to the aluminum-foil-covered copper plate collector. CA solution was spun in a Plexiglas humidity-control box (model, Plas Labs) with electrospinning parameters: 20-60% relative humidity, room temperature, 1.0 ml/hr solution flow rate, 15 kV applied voltage, and 12cm tip-to-collector distance. The nanoscale electrospun fibers were deposited onto the collector with random orientation to form a non-woven nanofibrous membrane. The resulting membrane was kept in 40°C oven overnight to remove residual solvent.

3.2.2. Regeneration of Cellulose

Deacetylation of the CA was achieved with 0.5N KOH in ethanol solution at constant shaking (50 rpm) at room temperature. After 3 hours, the hydrolyzed CA was rinsed with deionized water until pH paper confirmed neutral pH and placed in oven at 40°C overnight.

3.2.3. Alkyne Substitution

Adapted from Mangiante.[25] Nanofiber mats were added to IPA (12.75 ml/mmol CA; 48.5 ml/mmol RC) was added to the flask and let sit for 15 minutes. 5.1 wt% NaOH(aq) (40.0 ml/mmol CA; 4.25 ml/mmol RC) was added to the reaction mixture in 0.5 mL increments over 15 min to avoid chemically destroying the nanofibers. The reaction mixture was heated over one hour while shaking, and propargyl bromide (4.5 ml/mmol fiber) was

added via syringe. Temperature and shaking were maintained for specified time. Thin Layer Chromatography (TLC) was used to monitor reaction progress. 3:1 hexane to ethyl acetate was used as the developing solvent. For each sample removal, the flask was removed from water bath and let cool for 30 minutes. The nanofiber mat was rinsed with water, then IPA, then IPA/water mix, then sat in water for 10 minutes to ensure all unreacted materials had diffused from the mat. Lastly, the mat was dried in 40°C oven overnight.

3.2.4. Click reaction with biotin conjugate

Adapted from Celebioglu.[24] The azide-biotin-conjugate (1 equiv) was dissolved in 33.3 ml water per mmol fiber and the nanofiber mat was added to the solution. Fresh solutions of ascorbic acid (2.5 equiv, clear solution) and copper sulfate anhydrous (2.5 equiv, 34.67 mM, light blue solution) were prepared. The copper sulfate solution was added to the azide-biotin-conjugate solution first, then the ascorbic acid solution was added. The mixture shook at room temperature. After the specified time, the nanofiber mat was removed from the solution and rinsed with water and let soak in fresh water for three days to ensure all unreacted biotin diffused from the mat. The mat was rinsed briefly with water and dried in 30°C oven overnight.

3.2.5. Water Stability

Samples were immersed in DI water for 24 hours or 1 week. After drying at room temperature, samples were heated to 40°C or 80°C in oven for 24 hours. All samples

were conditioned in 65% RH conditioning room for 2 days before HABA colorimetric assay was performed.

3.3. Characterization

3.3.1. SEM and EDX

Fiber morphology and diameter were examined using scanning electron microscopy (Zeiss Gemini 500 SEM) with an accelerating voltage of 2 kV. ImageJ™ open source software (National Institutes of Health) was used to measure the mean fiber diameters. Fifty measurements were taken for each sample from three separate images. EDX spectra were collected with an accelerating voltage of 10 kV.

3.3.2. FTIR and Raman

The change in chemical structure was analyzed with FTIR spectroscopy (ATR-FTIR Spectrometer PerkinElmer Frontier) at each reaction step. Each spectrum was an average of 128 scans obtained between 4000 and 600 cm^{-1} at a resolution of 4 cm^{-1}. Four spectra were collected per sample. Alkyne substitution was confirmed with Raman spectroscopy (Renishaw InVia Confocal Raman microscope). Each spectrum was obtained between 3250 and 200 cm^{-1} with an excitation wavelength of 785 nm and a resolution of ~1 cm^{-1}. Three spectra were collected per sample.

3.3.3. XRD

The change in crystalline structure was analyzed with X-ray Diffraction (Bruker D8 Advance ECO powder diffractometer, 1 kW Cu-Kα source). Three spectra were collected per sample. Percent crystallinity was calculated based on 2θ intensities:

$$Cr\% = \frac{I_{002} - I_{am}}{I_{002}} * 100 \quad (3.1)$$

For cellulose II, the 2θ values for I_{002} and I_{am} are 21.7° and 16°, respectively.[28]

3.3.4. XPS

Samples were analyzed using a Scienta Omicron ESCA-2SR with operating pressure ca. 1x10-9 Torr. Monochromatic Al Kα x rays (1486.6 eV) with photoelectrons collected from a 2 mm diameter analysis spot. Photoelectrons were collected at a 0° emission angle with source to analyzer angle of 54.7°. A hemispherical analyzer determined electron kinetic energy, using a pass energy of 200 eV for wide/survey scans, and 50 eV for high resolution scans. A flood gun was used for charge neutralization of non-conductive samples. Degree of substitution of Azide-PEG3-biotin conjugate onto alkyne-RC nanofibers was calculated based on the ratio of sulfur to carbon obtained from the XPS scans:

$$DS_{XPS} = \frac{72.06 * \left(\frac{S}{C}\right)}{32 - \left(120 * \left(\frac{S}{C}\right)\right)} \quad (3.2)$$

3.3.5. HABA Colorimetric Assay

The surface available biotin was quantified using a competitive colorimetric assay kit. The absorbance was measured at 500 nm using a Lambda 35 UV/Vis Spectrophotometer from Perkin Elmer. The HABA/avidin solution was reconstituted in 100 µL of ultra-pure water, added to 1000 µL of 1x PBS buffer solution, and the absorbance was measured. A pre weighed piece of fiber mat was placed in the cuvette and shook for 3 minutes. The absorbance was measured with and without the fiber mat. The surface-available biotin was calculated using the following equation:

$$Surface\ Available\ Biotin\left(\frac{mg\ biotin}{g\ fiber}\right) = (A_{500}^{0} - A_{500})\left(\frac{MW_{biotin}V}{\varepsilon bW}\right) * 10^{3} \qquad (3.3)$$

where A_{500}^{0} is the absorbance of the solution prior to the addition of nanofiber mat; A_{500} is the absorbance of the solution after reaction with nanofiber mat; MW_{biotin} is the molecular weight of the biotin (244.3 g/mol);V is the volume of the solution (L); b is the cuvette path length (1 cm); ε is the extinction coefficient ofthe HABA/avidin complex at 500 nm (3.4x103L/(mol cm)); and W is weight of the surface shell of the fiber (g).

The surface available biotin was used to calculate the degree of substitution of biotin on the cellulose nanofibers:

$$DS_{HABA} = [Surface\ Available\ Biotin] * \frac{MW_{RC}}{10^{3} * MW_{biotin}} \qquad (3.4)$$

where MW_{RC} is the molecular weight of one anhydrous glucose unit (AGU) (162.14 g/mol).

3.3.6. Streptavidin-FITC binding and Confocal Microscopy

Static binding of streptavidin-FITC was carried out in a microwell plate. Mats were wet with PBS solution (0.300 ml) in a microwell plate overnight then let dry. 100 ul of 1uM strept-FITC solution per 0.70 mg of fiber was added to each well and the fiber mats soaked for 1 hour. Each mat was rinsed with PBS solution 3 times then placed in transportation containers to bring to confocal. Each mat was 4 mm x 4mm.

Bound streptavidin on the nanofiber surface was imaged using Zeiss LSM710 confocal microscope with water immersed 40x objective and 561nm laser.

4. RESULTS AND DISCUSSION

4.1. Formation of nonwoven nanofiber mats

4.1.1. As-spun cellulose acetate

The effect of binary solvent system and cellulose acetate (CA) concentration were previously reported to produce continuous smooth fibers without blocking the tip of the needle.[9] These parameters were used as the starting point for this study and adjusted based on preliminary experiments. The target relative humidity depended on whether an open (laboratory hood) or closed (glove box) system was used. Figure 4.1a shows the rough surface of the cylindrical as-spun fibers.

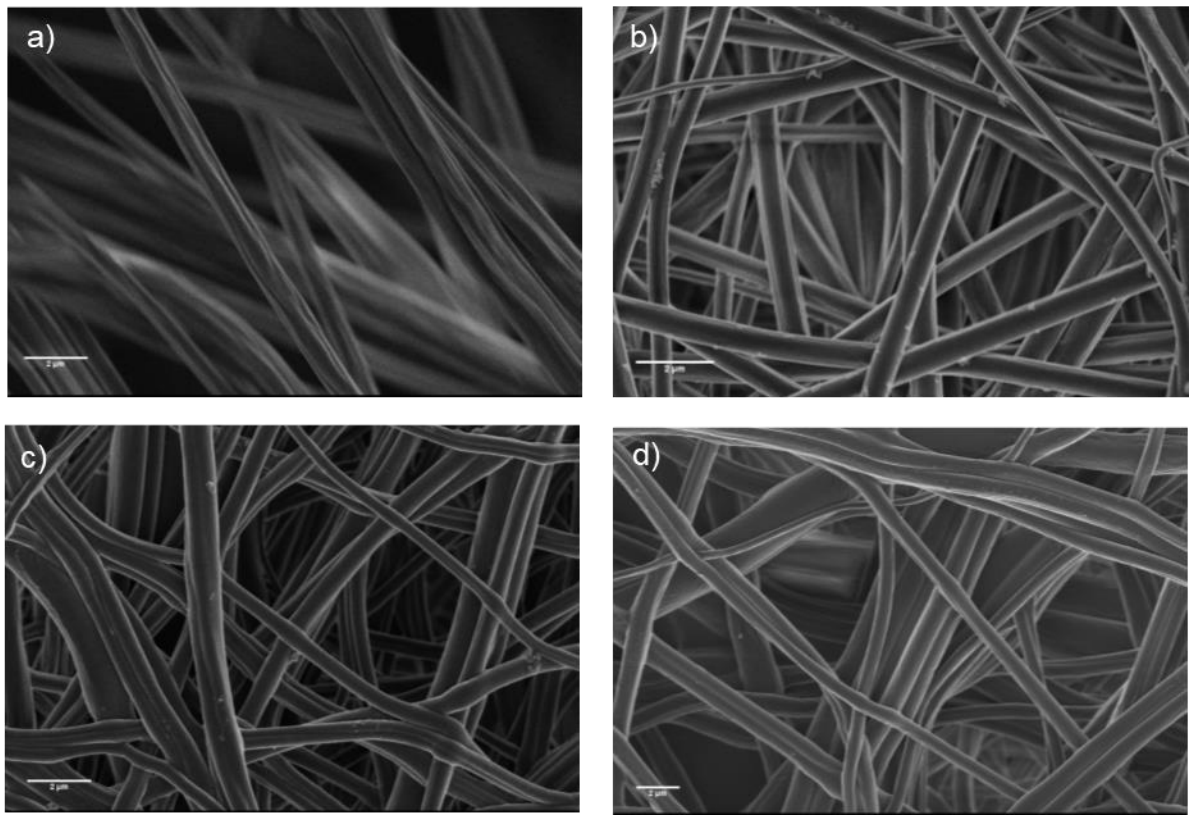

Figure 4.1: SEM images of a) as-spun cellulose acetate, b) deacetylated cellulose acetate, c) alkyne-cellulose, and d) biotin-cellulose nanofibers.

As previously reported, needle blockage and dried polymer accumulation on the tip of the needle were issues during spinning but were mitigated by occasionally dislodging the solid accumulation on the needle tip.[9,11,12,13,14] Temporary blockage caused side jets to form that reduced the diameter of the fibers. This resulted in a skewed distribution of fiber diameters seen in Figure 4.2 with a mean of 741 nm and median of 680 nm.

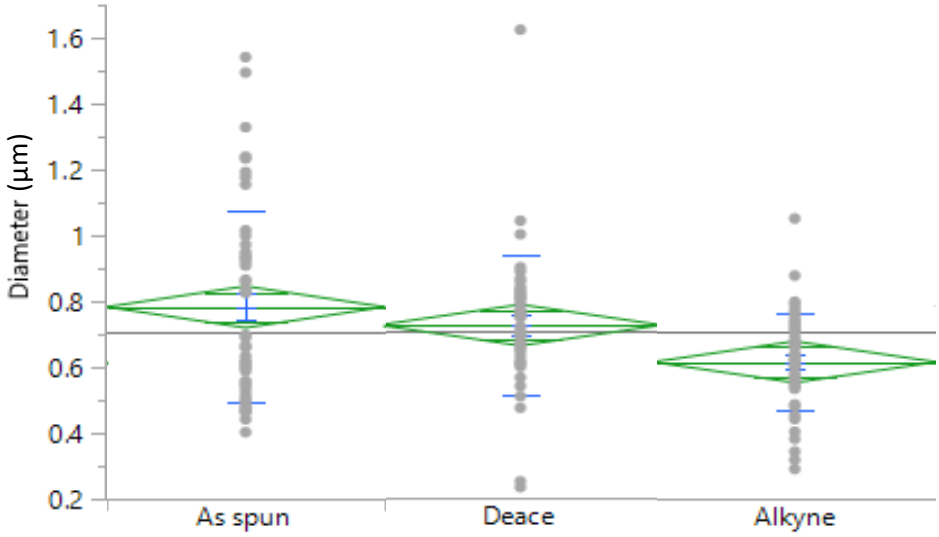

Figure 4.2: Fiber diameter distributions from SEM images for as-spun CA, deacetylated CA, and alkyne-RC

The relative humidity is thought to be the root cause of the surface roughness seen in Figure 4.1a. When spun in the glove box, lower relative humidity is required to produce fibers since the box is a closed system. The DCM and methanol evaporate during spinning, and they remain as vapors in the system. The buildup of their vapor pressures affects the evaporation rate of the electrospinning solution, and therefore, the spinnability of the fibers. Conversely, spinning in the hood is an open system where the circulation of the ventilation system removes the evaporated DCM and methanol and a higher RH is needed to maintain proper fiber formation. Clogging appears to be minimized in the 50-60% RH range with lower- to mid-50s being ideal. Less spurts and beads appear on the mat, and smoother, less fluffy fibers result. If the RH is too high, multiple jets develop: one cone will form then start to dry up, so another one will form out of the side then dry up, and the process will continue until the dried clump is dislodged from the needle. This

results in visibly finer fibers because the side jets are restricted by the surrounding dry clumps. Less solution can get through, so less mass is transferred and smaller diameters result. If too low RH, the spinning solution still dries on the tip of the needle, but multiple jets do not form. The extra moisture in the air at higher RH allows the spinning solution to stay partially moist so that the new solution being pushed through the needle can push past the partially solidified clumps. Whereas, with the too low RH, the spinning solution completely evaporates, and the dried clump clogs the needle tip, effectively gluing it shut and preventing new solution from exiting. Additionally, lower humidity produces fluffy fibers due to the buildup of static electricity in the drier air and on the drier fibers.

4.1.2. Regenerated cellulose

Cellulose nanofiber membranes were obtained by chemically deacetylating the as-spun cellulose acetate nanofiber membranes. After deacetylation, the cellulose nanofibers had a smooth, round structure shown in Figure 4.1b. The change in surface topography from as spun to deacetylated cellulose acetate was attributed to the reduction of surface energy while forming new hydrogen bonds between the newly formed hydroxyl groups. The average diameter of the cellulose acetate fibers from as spun to deacetylated was not significantly reduced, but Figure 4.2 shows that the distribution of diameters is narrows after deacetylation due to the removal of the acetyl groups.

The deacetylation of the CA nanofibers was confirmed by using FTIR spectra, shown in Figure 4.3.

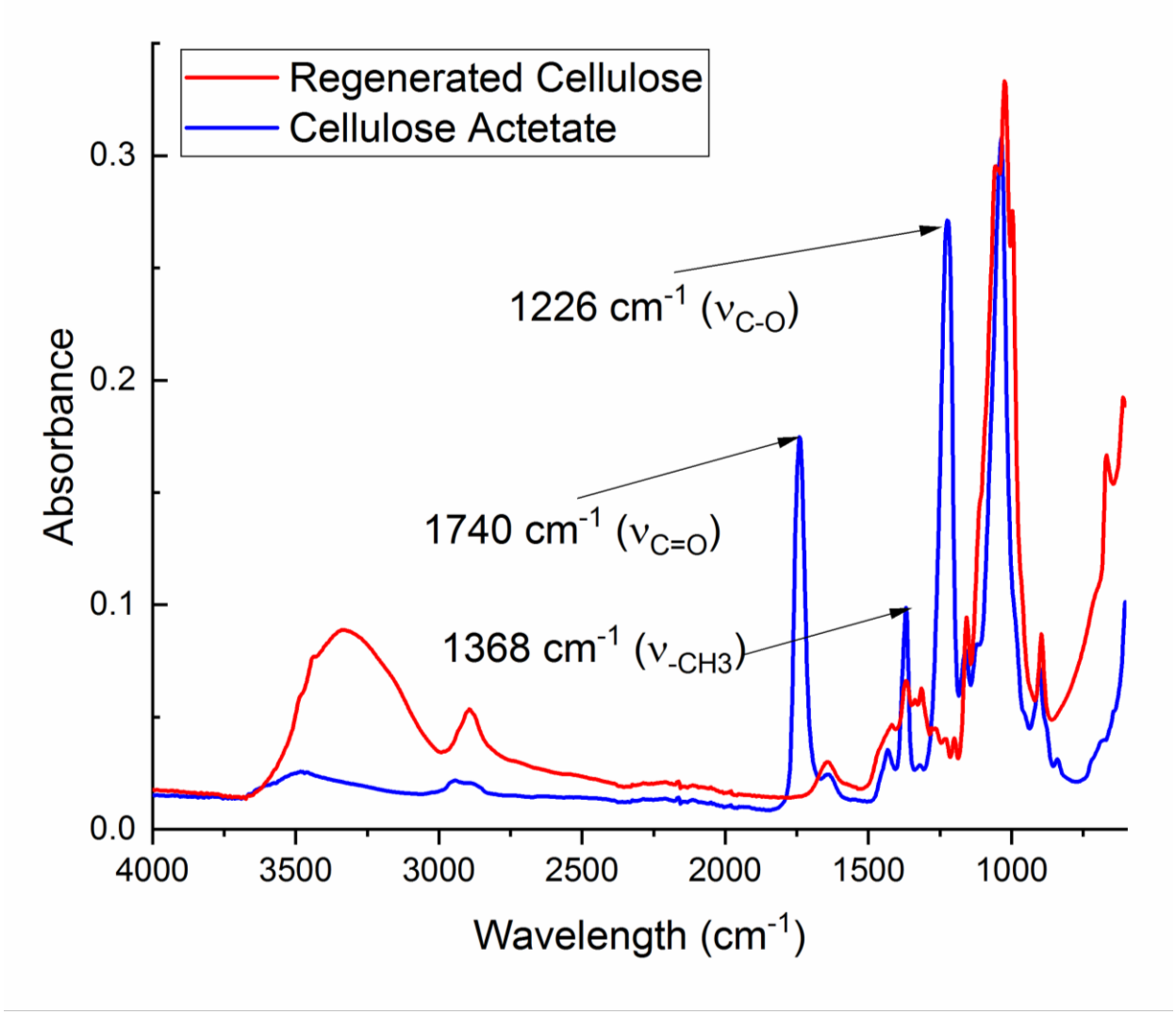

Figure 4.3: FTIR spectra of as spun and deacetylated CA nanofibers

The characteristic absorption bands for CA appear around 1740, 1226, 1368 cm^{-1} due to the C=0 and C-O stretching and C-H bending vibration of CH_3 of the acetyl group, respectively. The broad bands at 2850-2950 and 3400-3500 cm^{-1} are attributed to the C-H stretching of CH_2 or CH_3 and -OH stretching of unacetylated cellulose, respectively. The deacetylated CA show changes in these characteristic peaks to resemble native cellulose. Specifically, the disappearance of the 1740, 1226, 1368 cm^{-1} peaks and

increase in the 3100-3500 cm^{-1} band confirm the removal of the acetyl groups and exposure of the hydroxyl groups.

The as spun CA was deacetylated for 2 and 3 hours to ensure full deacetylation. FTIR and XRD was used to monitor the change in crystallinity and chain orientation after the reaction. For FTIR, the Lateral Order Index (LOI) and Total Crystallinity Index (TCI) were calculated for cellulose II from Equations 4.1 and 4.2 shown below.[10,28]

$$LOI = \frac{A_{1429\ cm^{-1}}}{A_{897\ cm^{-1}}} \quad (4.1)$$

$$TCI = \frac{A_{1372\ cm^{-1}}}{A_{2900\ cm^{-1}}} \quad (4.2)$$

LOI is the empirical crystallinity index that describes the overall order of the polymer chains. TCI more directly relates the amount of crystalline structure of cellulose to the amorphous region.[28] 1429 cm^{-1} is related to the CH_2 scissoring motion of the C6 group of the cellulose repeat unit. 897 cm^{-1} relates to the vibrational mode of C1 and its constituents. If the hydrogen bonding network is altered, then the 897cm^{-1} absorbance will reflect this.[10] 1372 cm^{-1} relates to C–H bending vibration of CH_3 in the acetyl group or C6. 2900 cm^{-1} relates to C-H stretching of CH_2 or CH_3. 1372 and 2900 cm^{-1} were chosen since they are not affected by changes in amount of water absorbed by the sample and not affected by change in lattice type.[10] However, 1429 and 897 cm^{-1} have similar intensities for amorphous cellulose and cellulose II. The LOI only differs if any cellulose I is mixed in. Since it is not possible for cellulose I to be present in this system, TCI was calculated in addition to LOI. Cellulose II does have a higher 897 cm^{-1} peak compared to amorphous cellulose, so if there is any difference in LOI between samples, then that is most likely a change in the internal order of the chains. Nelson and O'Connor showed this

by ball milling highly crystalline cellulose and tracked the XRD and FTIR over time. They found a correlation between ratio of amorphous/crystalline cellulose to both TCI and LOI. Higher LOI correlates to a higher ratio of amorphous to cellulose II whereas smaller TCI correlates to a higher ratio of amorphous to cellulose II.[28] Figure 4.4 shows that the overall order of the polymer chains increased with deacetylation, and that the crystallinity index of the regenerated cellulose increases with increasing reaction time.

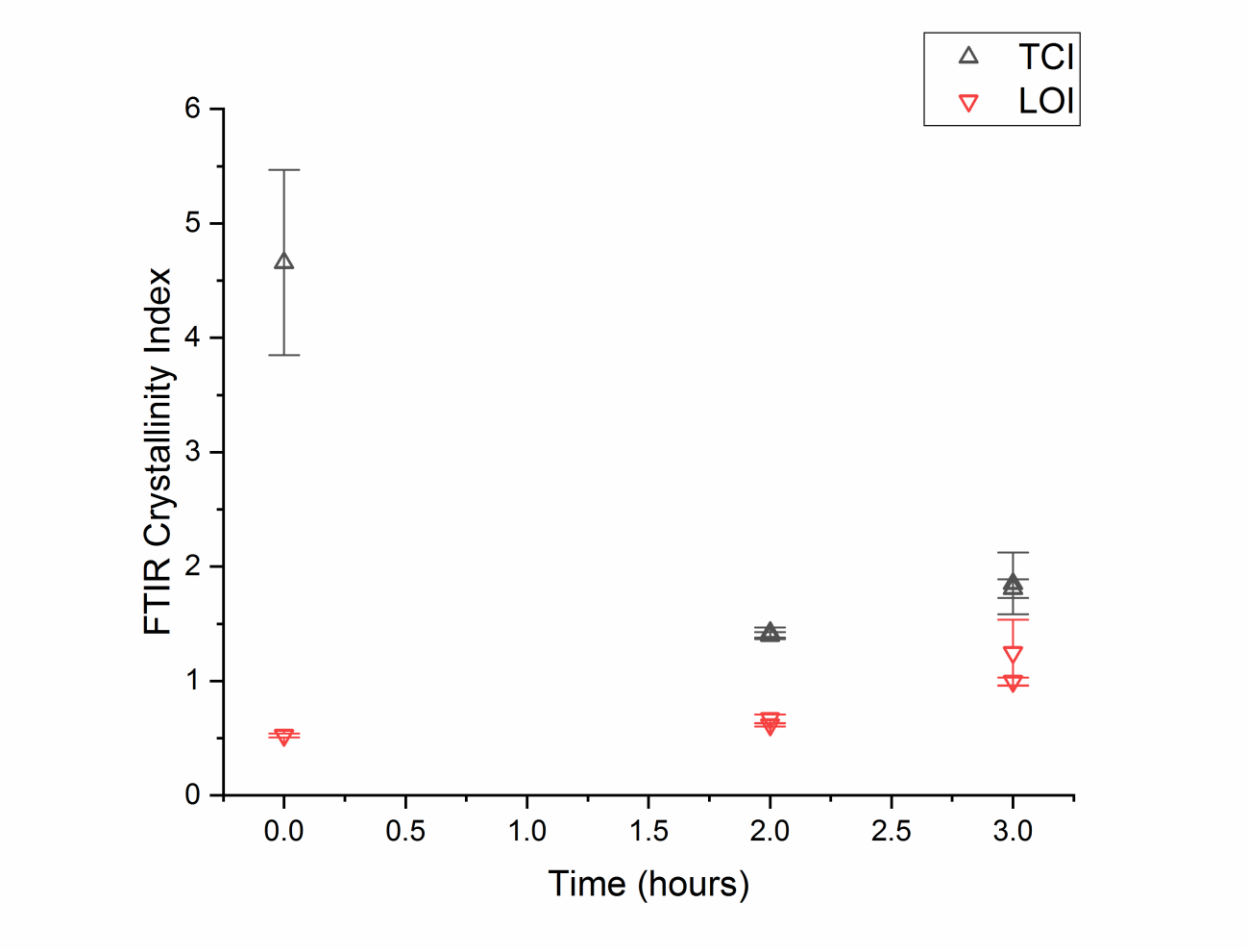

Figure 4.4: Total Crystallinity Index (TCI) and Lateral Order Index (LOI) calculated from FTIR spectra of as spun CA, 2 hour deacetylated CA, and 3 hour deacetylated CA shows that deacetylating for longer will increase the order of the cellulose chains of the nanofibers

As-spun cellulose acetate has high TCI due to the contribution of the CH_3 group in the acetyl groups to the C-H bending and stretching. Upon removal of the acetyl groups, only CH_2 groups are left in regenerated cellulose and the ratio reaches that of the typical amorphous cellulose. At longer deacetylation time, both the LOI and TCI increases. Higher TCI correlates well with higher orientation and more regular hydrogen bonding of the cellulose chains. The LOI trends are less clear and do not give strong indications, as predicted.

The FTIR is not an absolute measurement method, so the change in cellulose structure was also monitored using X-ray Diffraction (XRD). Various methods have been employed to quantify the Crystallinity Index (CI) from XRD data and are not necessarily cross-comparable between methods and studies. The Segal peak height method is the simplest method and thus, only provides relative values to be used for the purpose of comparing within the sample set only and is sufficient for our purposes.[29] After deacetylation of the cellulose acetate for 2 hours, the CI 55%. After an additional hour of deacetylation (3 hours total), the CI increased to 77%. The XRD CI confirms the increase in ordered cellulose structure seen in the FTIR data. Deacetylation not only removes the acetyl groups from the cellulose backbones, but also allows rearrangement of the inter- and intra-molecular hydrogen bonds to form the stable cellulose nanofibers.

4.2. Alkyne-grafted Cellulose Optimization

Alkyne-cellulose nanofiber membranes were obtained by S_N2 nucleophilic substitution of the propargyl groups to the surface hydroxyl groups of the cellulose acetate and

regenerated cellulose nanofiber membranes. At optimal conditions, the nanofibers maintained their morphology, shown in Figure 4.1c. A t-test shows that the alkyne-RC diameters were significantly reduced relative to both the as-spun and deacetylated CA fibers. Figure 4.2 shows that the alkyne-RC fiber diameter distribution has a smaller mean as well as smaller variance, which can be attributed to the sodium hydroxide treatment continue to reduce the fibers during the alkyne substitution reaction step and resulting in more uniformly distributed fiber diameters.

The alkyne substitution of the cellulose nanofibers was confirmed by using FTIR and Raman spectra, shown in Figure 4.5 and Figure 4.6, respectively.

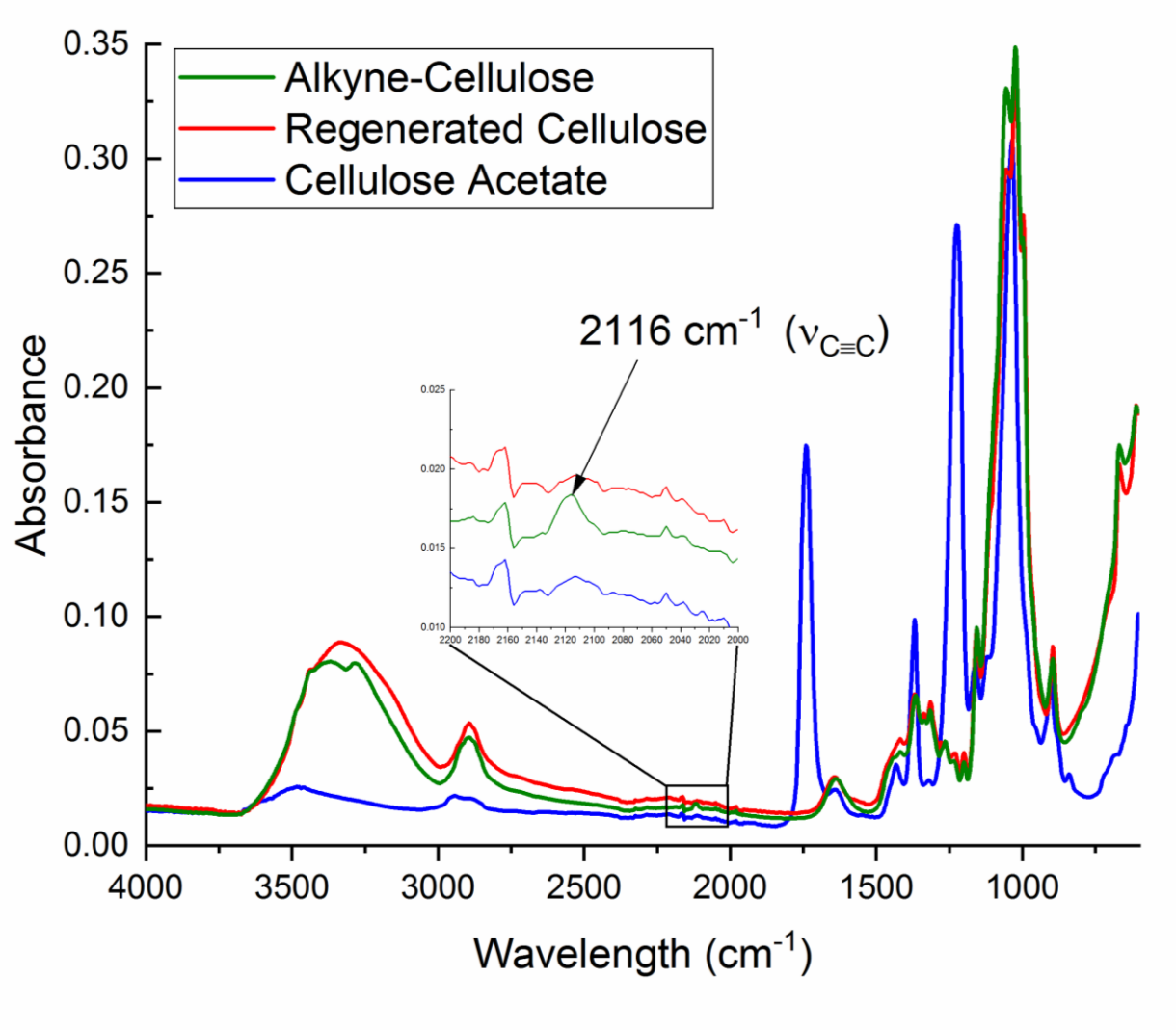

Figure 4.5: FTIR spectra of as-spun CA, deacetylated CA, and alkyne-substituted RC nanofibers

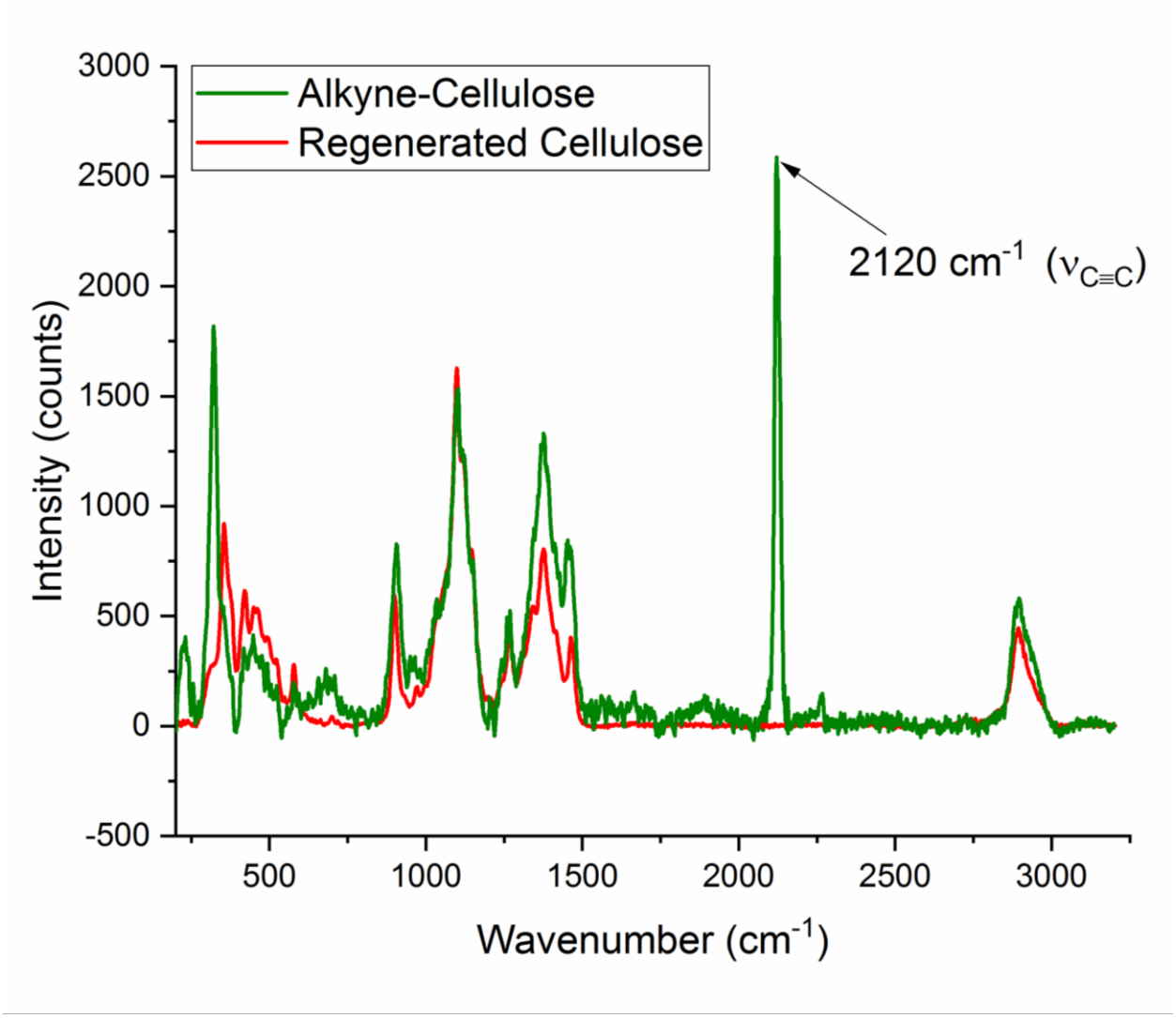

Figure 4.6: Raman spectra of deacetylated CA and alkyne-substituted RC nanofibers

Raman has less noise to signal compared to FTIR, which makes it easier to determine a background to the alkyne peak. The depth of penetration for FTIR and Raman are ~1 μm, so the spectra shows the average for the entire fiber. The spectra then would not reflect the surface availability of the alkynes, but the total availability. Alkyne groups on the surface of the fiber will be in low weight percent compared to all other vibrational modes of the cellulose polymer chains, but the relative intensities are dependent on the

spectroscopy technique used. The alkyne peak is small for FTIR even at high concentrations of the alkyne group, so for low concentrations it is difficult to differentiate the alkyne substitution from the background noise. Raman shows an intense, sharp peak for the alkyne group, so coupled with the low noise to signal ratio, Raman is a more reliable way to show that a sample contains an alkyne group. Raman is difficult to perform on nanofibers due to their curvature, and therefore, both FTIR and Raman spectroscopy was employed for the alkyne substitution. Care was taken to obtain reproducible spectra. Alkyne has low intensity peak for FTIR at 2116 cm^{-1} and high intensity peak for Raman at 2100 cm^{-1}. Changes in the sharpness of the broad band between 3100 and 3600 cm^{-1} confirm the change in the bonding of the hydroxyl groups and disruption of the hydrogen bonding. The ratio of the peak height of the alkyne group at 2115 cm^{-1} (FTIR) and 2100 cm^{-1} (Raman) to the reference peak of the ether bridge at ~1155 cm^{-1} was calculated to correlate the degree of alkyne substitution.

4.2.1. Solvent Ratio

Using the conditions from Mangiante, the solvent ratio used in the alkyne substitution reactions for CA and RC was determined from preliminary experiments.[25] 100, 80/20, 60/40, 40/60, 20/80, and 10/90 (v/v) water to isopropanol ratios were tested for 5.1 wt% NaOH in the aqueous solution addition. These ratios correlate to 5.1, 4.1, 3.1, 2.1, 1.1, and 0.5 wt% NaOH in total solution. In parallel, alkyne substitution reactions were carried out in 100% aqueous solution at the above-mentioned NaOH concentrations. The FTIR alkyne peak height ratios were calculated to compare the alkyne substitution within the sample set, shown in Figure A1 in the Appendix.

Mangiante used cellulose pulp in their experiments, so for those larger scale fibers it was advantageous to allow the fibers to swell first with the aqueous NaOH before adding IPA and heating the mixture. During the preliminary experiments of this study, both including and omitting the fiber swell step were tested, and higher alkyne substitution was found in the omitted fiber swell step trials, found in Figure A2. Therefore, this step was eliminated in all subsequent experiments.

Both water and IPA are polar protic solvents, which are not typical for S_N2 reactions due to the solvents hydrogen bonding with the nucleophile and interfering with the reaction. Polar aprotic solvents are not desirable for direct comparison between CA and RC systems since these solvents dissolve CA. Instead, the solvent effects were minimized by manipulating the remaining components. In the CA reaction systems, the sodium hydroxide deacetylates the CA in situ while also keeping the newly formed hydroxyl groups in their deprotonated form to facilitate the S_N2 substitution. The alkyne substitution is a concerted reaction that requires a strong nucleophile (deprotonated hydroxyl group) and unhindered electrophile (preferable a primary halide like propargyl bromide). The deprotonation of the hydroxyl groups is an equilibrium reaction and requires a high enough pH to maintain the alkoxide form. Therefore, with a decrease in the NaOH concentration, the pH decreases, the equilibrium favors the reactants, the hydroxyl groups are unavailable for nucleophilic substitution, and the alkyne substitution decreases. The hydroxide ions are used for the deacetylation reaction and not enough hydroxide is left over to carry out the alkyne substitution reaction. Too high of NaOH

concentration causes competing reactions to produce more byproducts such as propargyl acetate forming from the free acetyl groups. This is discussed further in the next section. The opposite is true for the RC hydroalcoholic reaction system. Since the RC is already deacetylated, the sodium hydroxide no longer has competing main reactions. With decreasing NaOH concentration, the side reactions are minimized due to multiple factors. First, the water concentration decreases, which decreases the rate of reaction of the side reactions involving water. One possible side reaction is the water undergoing substitution with the propargyl bromide. Since water only acts as a solvent in the propargyl bromide-RC substitution reaction, it is not a variable in the rate of reaction. Another factor that changes in the RC hydroalcoholic system is the concentration of IPA. Propargyl bromide is only slightly polar because the bromide has a 2.8 electronegativity and the carbon has a 2.5 electronegativity. The difference is not large enough to be polar or ionic, so propargyl bromide is slightly polar covalent. Therefore, propargyl bromide is only slightly soluble in water. IPA is polar and completely miscible with water; the secondary alcohol hydrogen bonds with the surrounding water molecules. It also has the carbons angled away from the alcohol group, allowing for the carbons in the propargyl bromide to interact with the London dispersion forces. With the addition of IPA, propargyl bromide can be more dispersed throughout the reaction solution and participate in the alkyne-RC substitution reaction. IPA has a dielectric constant of 17.9 and water is 80.1, so the water can dissolve more ionic compounds than IPA. During the substitution reaction, Na^+ and Br^- are formed and can be dissolved in the water present. Likewise, the water will more readily dissolve the sodium hydroxide than the IPA. This is a quasi-binary-phase reaction system with IPA acting as a phase transfer facilitator. The NaOH is more soluble in water than IPA, but a

small amount of the NaOH will reside in the IPA. This allows for the CA or RC to interact with both the water phase and IPA phase with a gradient of NaOH concentration. This not only facilitates the nucleophilic substitution reaction, but also protects the sample from being degraded.

The impact of the IPA additions is confirmed by the same RC reaction conditions being run with only aqueous NaOH. The same overall wt% of NaOH was used, but IPA was omitted. This reaction system had a sharp decrease in alkyne substitution with decrease in NaOH concentration due to the propargyl bromide and hydroxide ions not being able to interact in only water solution. Therefore, IPA is crucial in facilitating a successful alkyne-RC substitution reaction.

4.2.2. Temperature and Time

The nucleophilic substitution of the alkyne group onto the nanofiber surface was tested at three levels of temperature and six time intervals for both CA and RC. The ratio of the FTIR peak height of the alkyne group at ~2115 cm^{-1} to the reference peak of the ether bridge at ~1155 cm^{-1} and the ratio of the Raman peak height of the alkyne group at ~2100 cm^{-1} to the reference peak of the ether bridge at ~1155 cm^{-1} were calculated to correlate the degree of alkyne substitution to reaction condition, shown in Figure 4.7.

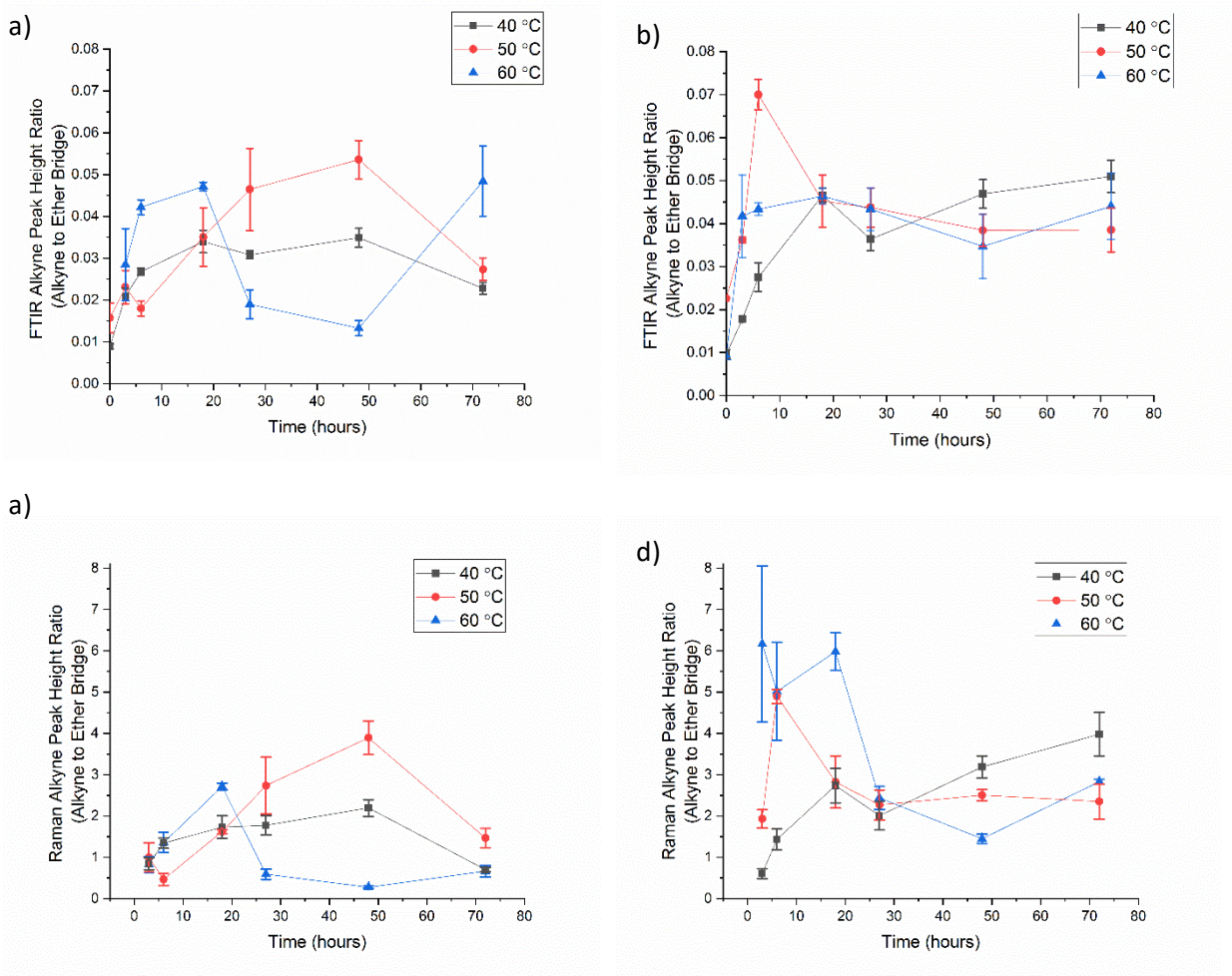

Figure 4.7: Alkyne substitution reaction yield as a function of temperature and time compared using a,b) FTIR and c,d) Raman spectra's alkyne peak height ratios for a,c) cellulose acetate and b,d) regenerated cellulose nanofibers

For the CA trials, the carbonyl peak of the acetyl group disappears in the FTIR spectra within the first 3 hours. The calculated peak height ratios are relative but show trends in the alkyne substitution. The FTIR and Raman data follow the same trends for all trials except for the RC at 60C. This trial exhibited a high peak height ratio and high spread for the 3-hour Raman, which was unusual for all other trials, i.e. all other trials started with a low substitution at 3 hours and increased over time before reaching a maximum and subsequently decreasing the peak height ratio. This maximum was due to the tradeoff

between the nucleophilic substitution of the alkyne group, other competing reactions, and degradation of the nanofiber mat. The Raman shows that as the reaction progresses (3 to 18 hours), the standard deviation decreases, and the fibers become more uniformly substituted. After 18 hours, hydrolysis of the glucose units results in loss of the alkyne substitution and a decrease in the alkyne peak ratio. Degradation was monitored by total weight change of the samples before and after the reaction, shown in Table 4.1 below. The control was subjected to the reaction conditions for 72 hours without the PBr addition.

Table 4.1: Weight loss of alkyne substitution reaction samples for RC and CA compared to PBr-free control

	Initial Weight (mg)		Percent Weight Loss (%)		
Sample	Mean	Std Dev	Mean	Std Dev	Control
40C - RC	13.0	2.5	4.6	6.0	39.7
40C - CA	17.9	2.5	41.6	3.2	44.6
50C - RC	10.2	2.6	10.2	10.2	89.8
50C - CA	21.5	1.5	40.7	5.1	52.7
60C - RC	8.1	1.3	1.9	7.3	89.0
60C - CA	12.4	2.1	50.5	19.2	100.0

CA total weight change is dependent on acetyl removal and glucose unit hydrolysis contributions. The CA weight loss from polymer chain degradation cannot be isolated, but the major contribution of the total weight loss seen for CA can be attributed to the acetyl removal. Both RC and CA systems have higher weight loss for the control sample versus the reaction sample. The control confirms that both RC and CA are susceptible to alkaline attack of the cellulose units, and that increasing the temperature accelerates the degradation rate. With handling and weighing small sample sizes as well as uncontrolled changes in moisture absorption, the weight loss measurements can only give a rough estimate towards sample degradation.

TLC plates were used to indirectly monitor the alkyne substitution reaction progress by sampling the reaction solution. The TLC plates showed that propargyl bromide remained in excess as the corresponding spot did not disappear for all reaction time and temperatures for both RC and CA. The effect of temperature can be seen for both the CA and RC trials. The 40°C trials consistently had the lowest alkyne substitution due to lower available energy in the system and therefore, slower reaction rate of the nucleophilic substitution of propargyl bromide. Since elimination reactions favor higher temperature, the lower temperature also decreased the rate of the competing reactions. This was evident in the TLC plates where the byproducts dissolved in the reaction solution gained a high enough concentration only at longer reaction times for 40°C compared to the higher temperatures. TLC plates from the CA trials revealed byproducts earlier in the reaction as well as more types of byproducts compared to the RC trials. Possible byproducts were identified as propargyl alcohol and propargyl acetate. Propargyl acetate was not seen on the RC TLC plates, as the free acetate groups were only formed in the CA reactions. Other byproducts that appeared on the TLC plates were not identified but were possibly byproducts from degradation reactions. Amorphous cellulose is susceptible to alkaline degradation even at low temperatures and hydroxide concentrations, but no evidence of major chemical degradation (chain scission, oxidation, etc.) or formation of aldehyde, carboxyl, or carbonyl groups was seen in the FTIR spectra for all reaction temperatures and times.[30] In addition, FTIR did not show evidence of the alkyne groups reducing to alkene or alkane once attached to the cellulose unit. The degradation products could be visualized on the TLC plates as direct products or used as an intermediate for subsequent product formation as other

spots on the TLC plates. A more direct characterization is required to identify all dissolved byproducts in the reaction solution. Visible degradation with the naked eye was observed for the 40°C, 50°C, and 60°C trials for CA samples starting at 18, 18, and 6 hours of reaction time, respectively: decreased density of the nanofibers in areas of the mats, yellowing/browning of the nanofibers, and holes from complete degradation of nanofibers. Slight yellowing was observed for the 60°C trials for RC samples starting at 27 hours, but no other visible degradation with the naked eye was observed for RC samples. Visible degradation was also observed in the SEM images. Onset of degradation is 27 hours for CA, with major degradation seen in 72-hour sample. RC morphology of smooth fibers with little visible degradation is retained throughout the 72 hours of reaction time. In addition, the CA mats had less dimensional stability than the RC mats.

It is important to note that the CA is deacetylated in situ, which can partially explain the instability of the CA nanofibers during the reaction. Figure 4.8 illustrates the differences in the reaction mechanisms for the CA and RC reactions. Alkalization mechanism investigation in IPA-water-sodium-hydroxide-cellulose system was previously reported by Yokota and used as basis for the proposed mechanisms for CA and RC alkyne substitution.[31] A higher amount of sodium hydroxide was required in the CA trials in order to remove the acetate groups from the nanofiber as well as act as base in the nucleophilic substitution reaction. With the low ratio of isopropanol, the CA nanofibers were in higher contact with sodium-hydroxide-rich aqueous phase even with vigorous stirring. Since the isopropanol was in a much smaller ratio, the CA reaction conditions gave rise to a higher amount of alkaline degradation and lower alkyne substitution. In

the RC trials, the high ratio of isopropanol allowed for the propargyl bromide to be fully soluble in the isopropanol phase and the sodium hydroxide was rich in the aqueous phase. Under vigorous stirring, the aqueous phase was dispersed as fine droplets in the isopropanol phase since the reaction solution was mostly isopropanol. The nucleophilic substitution reaction occurred on the RC fibers when they were mostly in contact with the isopropanol phase, which had the lower concentration of sodium hydroxide. The isopropanol acted as a protecting agent so that the RC fibers were not degraded by the sodium hydroxide, and so that the sodium hydroxide was only used for its intended purpose of aiding in the nucleophilic substitution reaction.

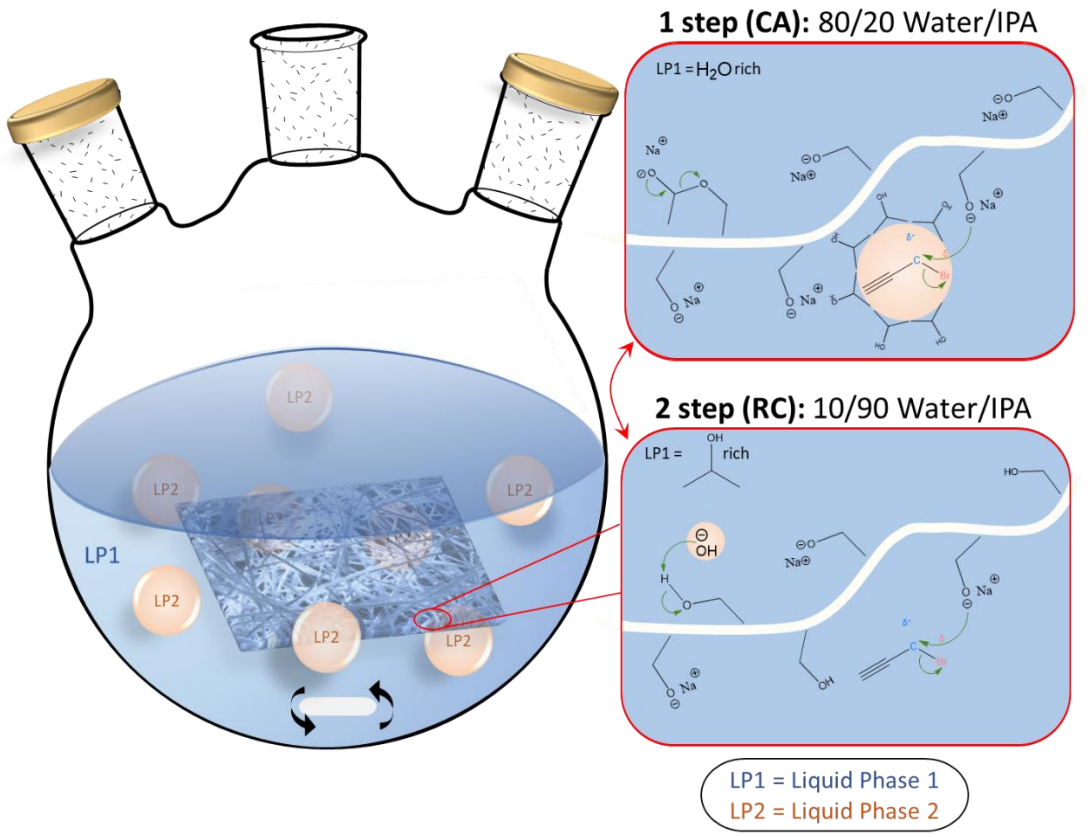

Figure 4.8: Schematic of proposed alkyne substitution reaction for a) CA nanofiber membranes with higher ratio of sodium-hydroxide-rich phase and b) RC nanofiber membranes with higher ratio of propargyl-bromide-rich phase

It is also important that almost all the no-PBr controls were barely unrecoverable after 72 hours. This underscores the importance of balancing the amount of PBr and NaOH added to the reaction solution. Without the PBr for the sodium hydroxide to interact with, the sodium hydroxide attacks the CA and RC and degrades the polymer chains through chain scission and/or oxidation. With PBr in excess, the sodium hydroxide is devoted to aiding in the nucleophilic substitution reaction and other competing reactions, but less devoted to polymer chain degradation.

The crystallinity and order of the cellulose chains were monitored via FTIR, as described in Section 4.1.2. Figure 4.9 shows that overall, the reaction does not disrupt the order of the cellulose chains. TCI for initial CA is 4.66.

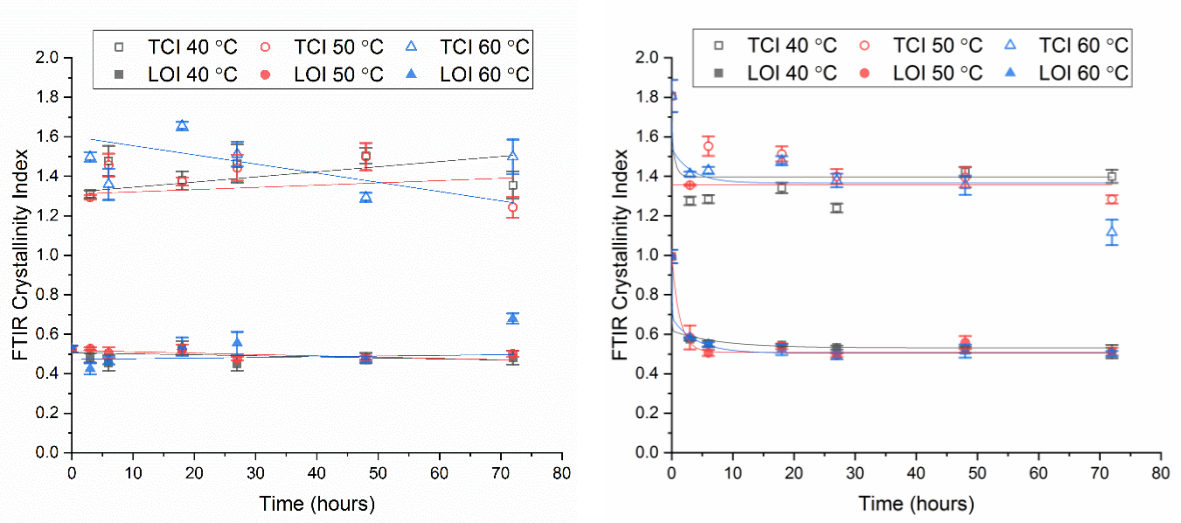

Figure 4.9: LOI and TCI calculated from FTIR spectra for a) cellulose acetate and b) regenerated cellulose nanofibers. After the initial drop, the change in crystallinity and order of polymer chains do not change significantly during the alkyne substitution reaction.

Change in TCI and LOI during the alkyne substitution reaction does not necessarily correlate to a change in crystallinity. The propargyl bromide will substitute onto the C6 first. This will affect the adjacent CH2 groups bending, stretching, and scissoring motion; all represented in the TCI and LOI ratios. Even so, there is negligible difference between both ratios with increasing reaction time. Small standard deviations further justify the use of FTIR and these ratios to relate the change in the cellulose inter- and intra-molecular bonds.

Once deacetylated, the RC nanofibers do not rearrange (increase crystallization or lattice orientation) due to the alcohol acting as an anti-swelling agent. Even in the control without propargyl bromide to react with the sodium hydroxide, the crystallinity/order indicators do not significantly differ from the reaction samples. Instead of the sodium hydroxide breaking hydrogen bonds and allowing rearrangement of the molecular chains, the sodium hydroxide may be participating in other reactions such as scission of the polysaccharide chains. Also, the heat treatment of the fibers can also influence the change in crystallinity. Initial decay in RC trials shows the removal of any crystallinity imparted during the deacetylation step with a sharp increase in the TCI of the 50 C trial at 6 hours correlating with the maximum alkyne substitution seen in Figure 4.7b,d.

XRD was used to characterize the change in crystalline structure during the alkyne substitution reaction. Based on the FTIR and Raman results, only the 50°C samples were characterized with XRD. Figure 4.10 shows that after the initial transition of both CA and RC to the amorphous cellulose within the first three hours of the alkyne substitution reaction, the order of the cellulose chains is maintained throughout the reaction time.

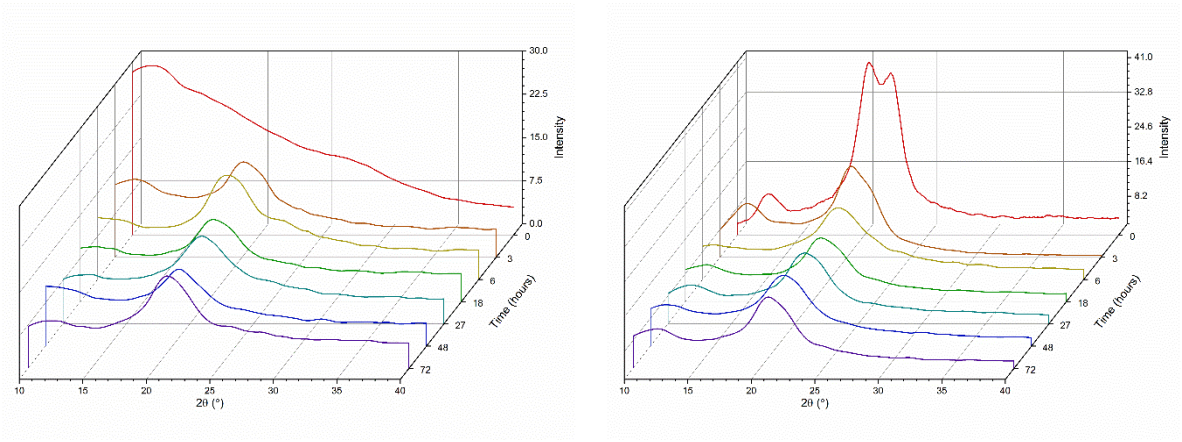

Figure 4.10: XRD plots of a) CA and b) RC during the alkyne substitution reaction. The hydroalcoholic NaOH initially alters the structure of the polymer chains until an equilibrium structure is reached.

The RC begins with relatively sharp peaks resembling cellulose II crystalline regions at 20.3° and 21.7°. The RC sample after 3 hours still has a slight shoulder at the 21.7° position, indicating the hydrogen bonding network between cellulose chains take longer to break and reform in the RC reaction system due to the smaller concentration of NaOH and phase transfer solvent of IPA. After 6 hours, the RC reaches its equilibrium orientation and maintains this state for the remainder of the reaction. These trends were confirmed by quantifying the crystallinity index using the previously described Segal method, shown in Figure 4.11.

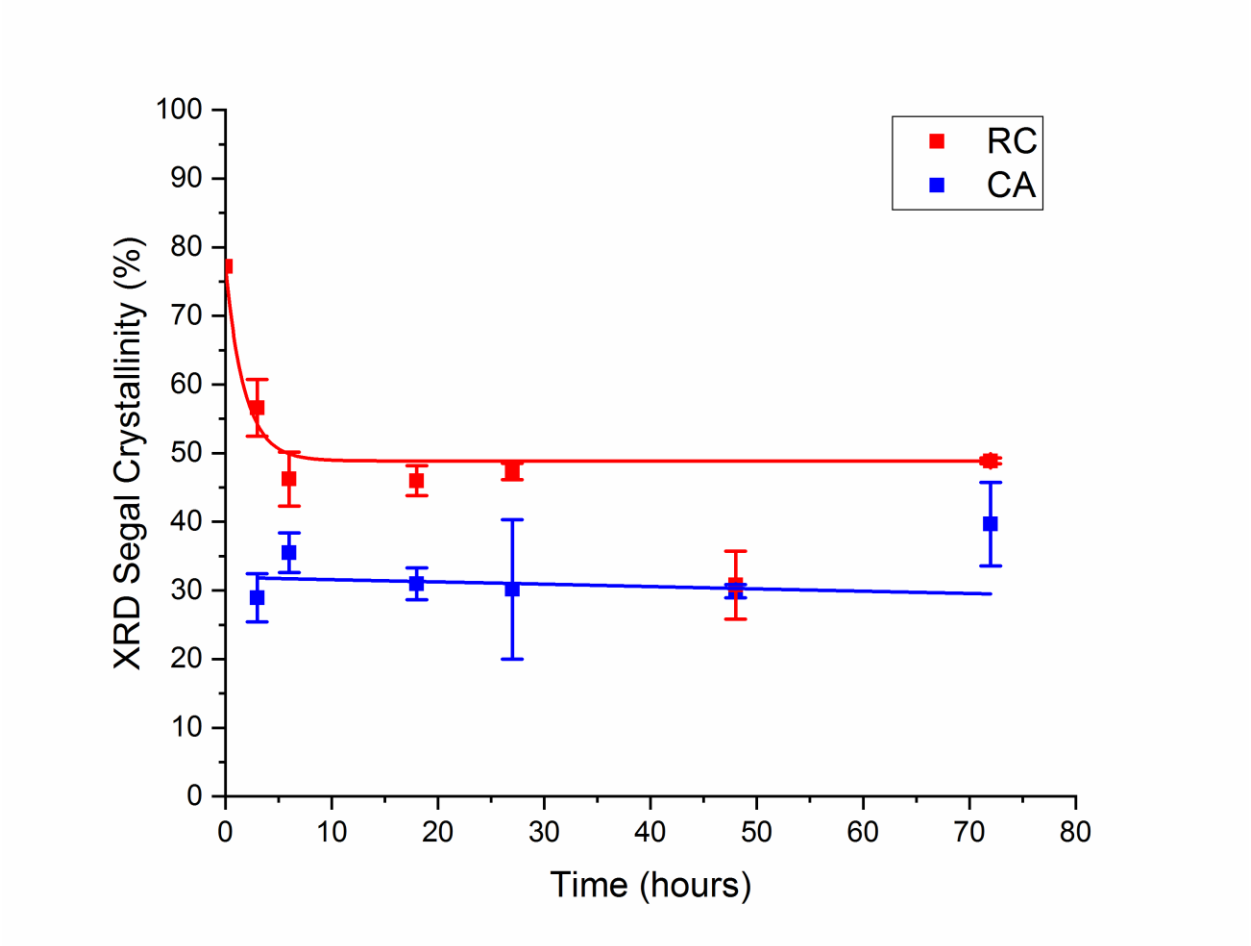

Figure 4.11: Crystallinity Index from XRD data for RC and CA during alkyne substitution reaction. After the initial decay, both RC and CA reach equilibrium states of chain structure.

Figure 4.11 shows that the amount of order obtained during deacetylation was lost with increase in reaction time until an equilibrium is reached for RC, and that the amorphous as-spun CA transitions into regenerated cellulose as the reaction proceeds. The CA also reaches an equilibrium. This is consistent with the FTIR crystallinity indices and confirms that the reaction only takes place at the surface and that the bulk of the fiber is unaffected.

RC is dimensionally stable enough to move on to the click reaction step. The CA mat is not stable enough to warrant continued functionalization. A thicker mat might mitigate the

issue of holes being “burned” by the sodium hydroxide, but that method would still be less effective than the two-step (RC) method. Regenerating the mat then substituting the mat is a safer, milder process that reduces the overall reaction time from 48 hours to 8 hours.

Final conditions chosen for alkyne substitution are RC in 20/80 IPA/water at 50°C for 6 hours.

4.3. CuAAC Click Reaction

Alkyne-substituted RC mats and azide-biotin-conjugate participated in the copper(I)-catalyzed alkyne-azide cycloaddition (CuAAc) click reaction. Copper (II) sulfate was used as the source of copper, and ascorbic acid acted as a reducing agent to reduce copper (II) to copper (I). The copper (I) subsequently catalyzed the click coupling of the alkyne attached to the nanofiber mat and the azide attached to the biotin conjugate to form the triazole ring that links the biotin to the cellulose nanofibers. 2, 5, and 10 equiv of ascorbic acid to copper sulfate were tested alongside six controls in the following permutations listed in Table 4.2 below to elucidate the interactions of each component with the nanofibers.

Table 4.2: Click reaction sample components

		Click Reaction Components			
Role		Click Molecule		Catalyst	
Chemical		Alkyne-RC	Azide-Biotin	$CuSO_4$	Ascorbic Acid
Reaction		X	X	X	X
Control	1		X	X	X
	2		X	X	
	3	X		X	X
	4	X	X		X
	5	X	X	X	
	6	X	X		

At all click conditions, the nanofibers maintained their morphology, shown in Figure 4.1d. A One-way ANOVA test was run on all sample's fiber diameters with distributions shown in Figure 4.12. With a probability of less than 0.001, the null hypothesis of all the mean diameters being equivalent is rejected.

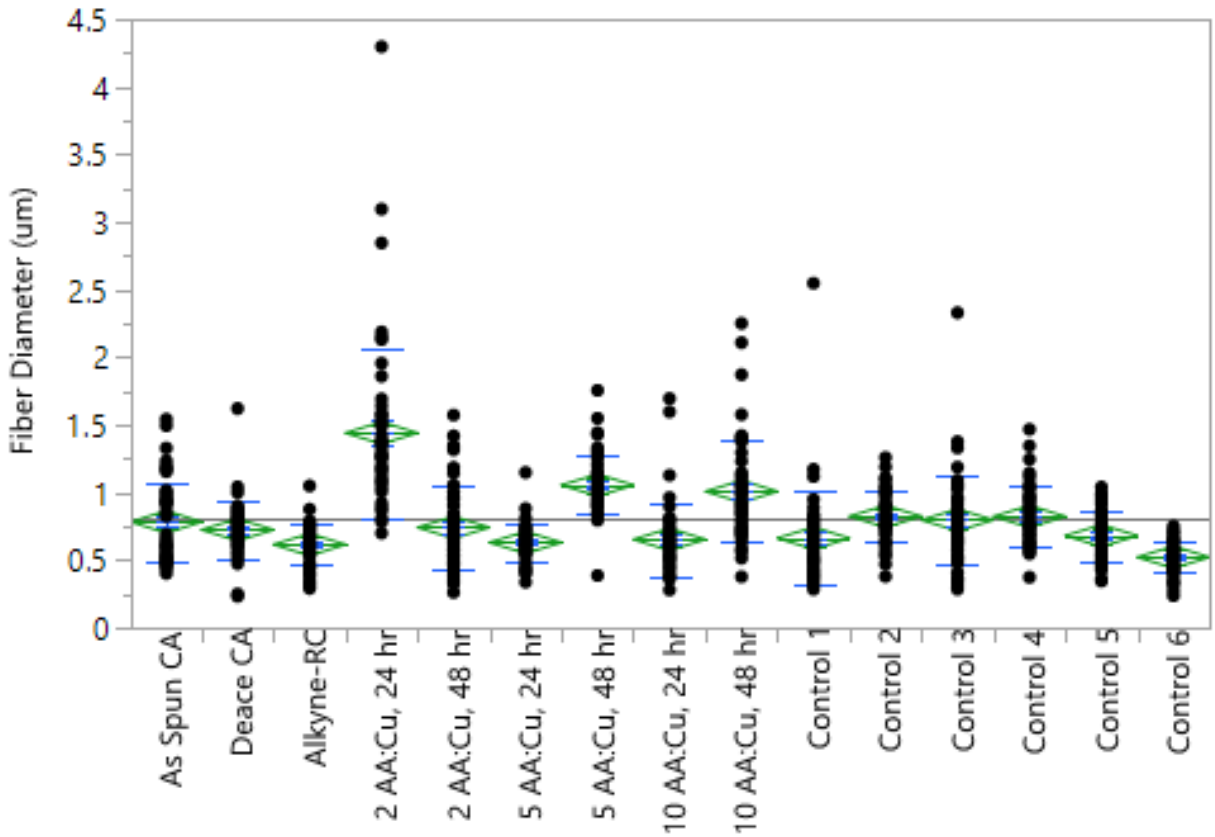

Figure 4.12: Fiber diameter distributions from SEM images of click reaction samples show that the click reaction does not a significant effect on fiber diameter determination

A Posthoc Multiple Comparison with Tukey Correction was performed to determine which samples were significantly different from the initial alkyne-RC. Table 4.3 shows that there is no trend between successful click reactions and significant change in fiber diameter. Therefore, the biotin addition is not the only factor in the change of fiber diameter. The cellulose fiber swells in the aqueous solution, and the swelling can cause rearrangements in the inter- and intramolecular hydrogen bonding which can result in the collapse of the fiber or a sustained swelling upon removal of the water.

Table 4.3: P-value results from Multiple Mean Comparison with Tukey Correction of click reaction samples versus initial alkyne-RC fibers

Diameter of Sample vs Alkyne	P<0.05	P>0.05
2 AA:Cu, 24 hr	X	
2 AA:Cu, 48 hr		X
5 AA:Cu. 24 hr		X
5 AA:Cu. 48 hr	X	
10 AA:Cu, 24 hr		X
10 AA:Cu, 48 hr	X	
Control 1		X
Control 2	X	
Control 3		X
Control 4	X	
Control 5		X
Control 6		X

The biotin substitution of the cellulose nanofibers was confirmed by using FTIR spectra, shown in Figure 4.13.

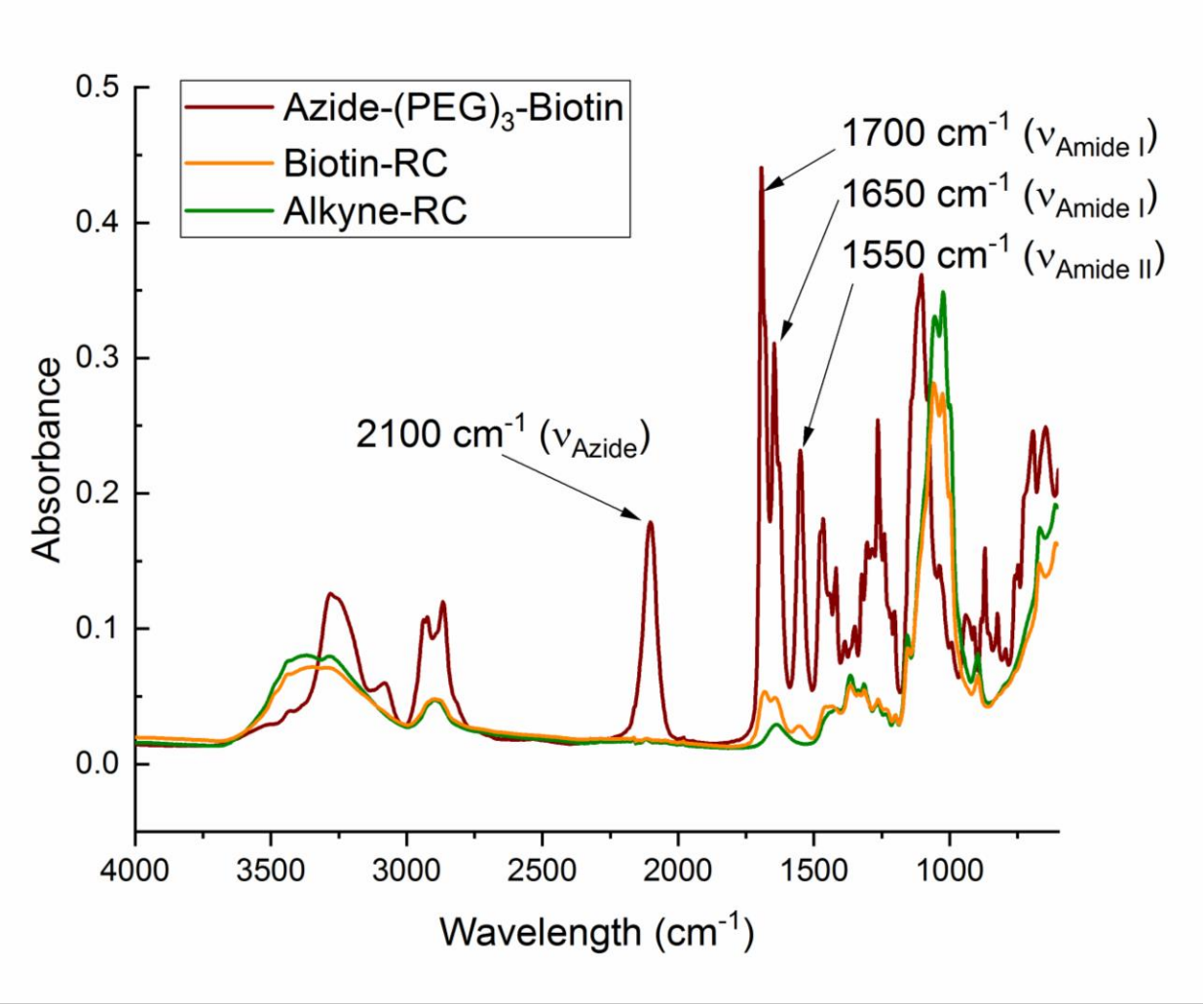

Figure 4.13: FTIR spectra of alkyne-RC, biotin-RC, and azide-PEG3-biotin conjugate

The characteristic absorption bands for the biotin conjugate appear around 1700, 1650, and 1550 cm^{-1} due to Amide I and II of the carbamide of biotin and amide of the peptide linkage of biotin to PEG section of the conjugate. Amide I band is due to C=O stretching vibrations of the peptide bonds whereas the Amide II band is due to C-N stretching vibrations in combination with N-H bending. The azide group in the biotin conjugate at

2100 cm^{-1} disappears after the click reaction, but the 1700, 1650, and 1550 cm^{-1} peaks remain in the successfully clicked samples. These characteristic peaks were used as the first indication for successful click reaction. Figure 4.14 shows that all samples with all reaction components (varying ascorbic acid to copper sulfate ratio) and Control 5 gain biotin peaks whereas the remaining controls do not show evidence of biotin.

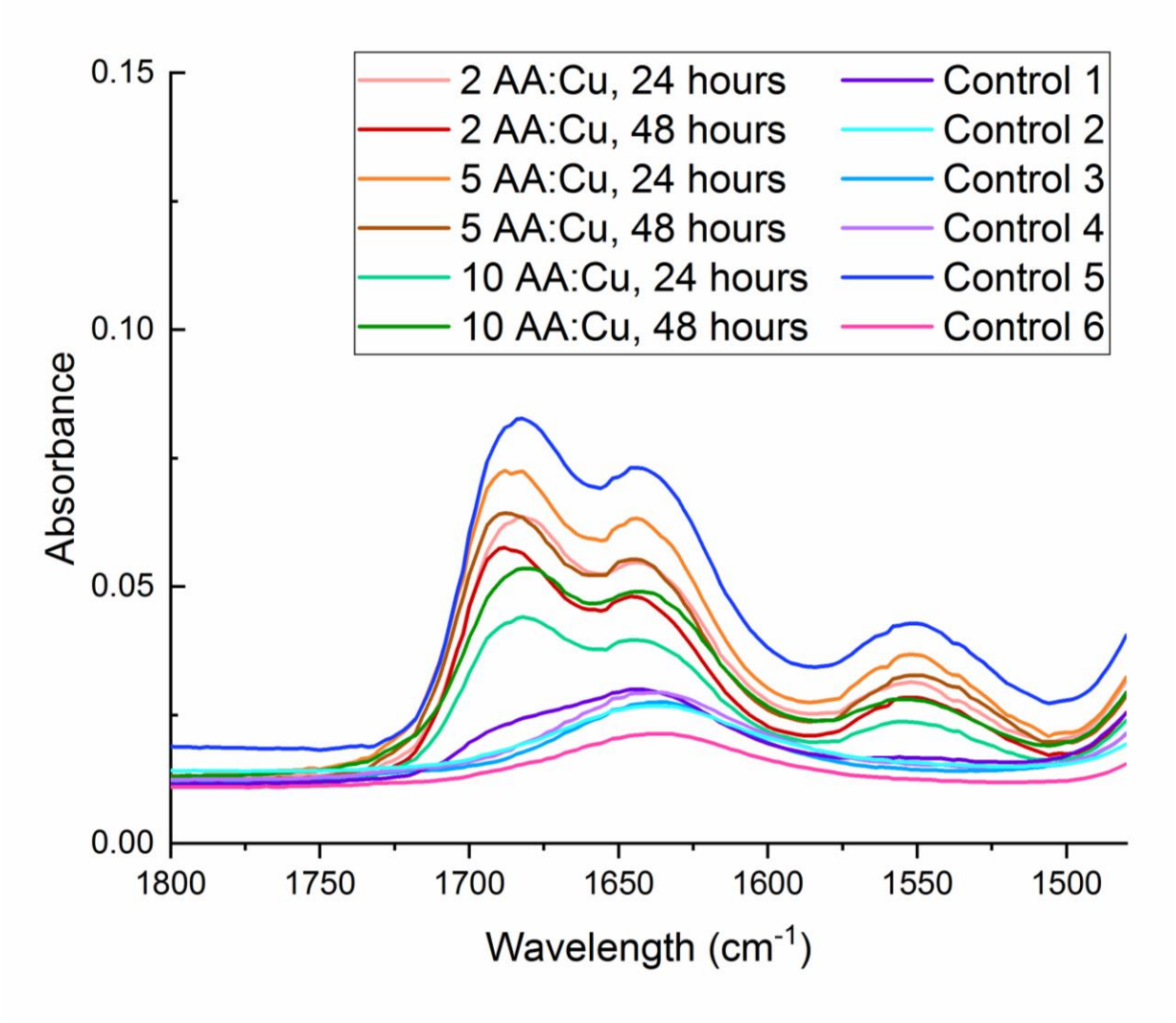

Figure 4.14: FTIR spectra of biotin-RC samples for various reaction conditions

4.3.1. EDX

Elemental mapping was used to analyze the distribution of biotin. Sulfur and nitrogen are both unique to the biotin conjugate except for potential residual sulfur from the sulfate ions of copper sulfate. Figure 4.15 shows a representative example of the elements analyzed.

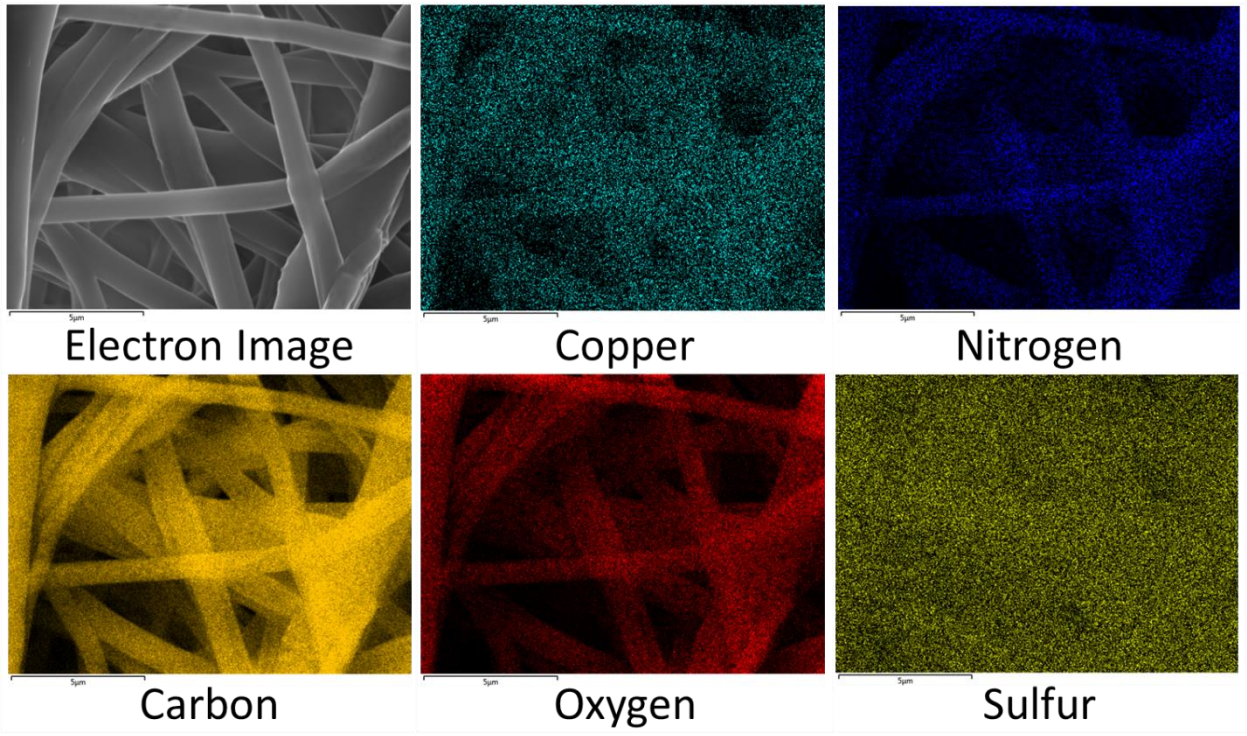

Figure 4.15: Elemental mapping from EDX of biotin-RC fibers

The carbon and oxygen are both present in the cellulose nanofibers as well as the biotin conjugate. Nitrogen, only present in the biotin conjugate, is seen along the fibers and not in the interstitial spaces. This confirms that the biotin conjugate is not simply just entangled in the pores of the membrane but immobilized on the surface of the nanofibers. The nitrogen along the fibers is consistently seen in all the same trials as

the ones with biotin FTIR peaks. No nitrogen was detected for the remaining samples. Residual copper is observed in all alkyne-RC trials. In Control 1, copper sulfate was included in the reaction mixture, but no copper was detected in the elemental mapping. The copper coordinates with the alkyne during the first step of the click mechanism, so residual copper will remain bound to unreacted alkyne after the reaction as well as coordinating with the newly formed triazole ring. If no alkyne or triazole rings are present, the copper will not coordinate strongly enough to any other components in the system. Sulfur is observed in all samples, even ones that did not encounter copper sulfate (eg. initial alkyne-RC and Control 6). Therefore, background noise convolutes the sulfur map, and nitrogen is the better indicator for successful biotin immobilization.

4.3.2. Streptavidin-FITC Binding

For the biotin-cellulose nanofiber membranes to be used in a diagnostic device, the membranes must be able to selectively and rapidly bind streptavidin. Fluorescently tagged streptavidin was used as the model binding molecule. The binding schematic is shown in Figure 4.16 below.

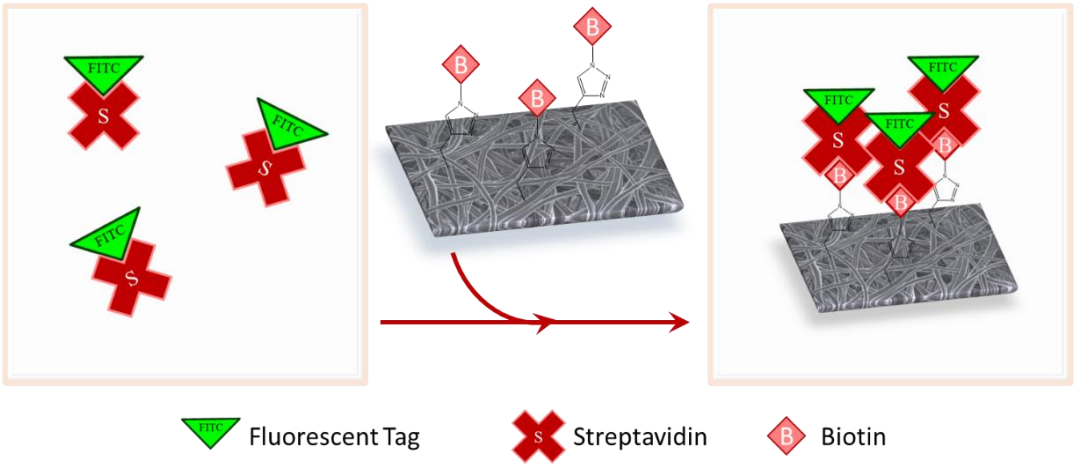

Figure 4.16: Strepavidin-biotin binding schematic: fluorescently tagged streptavidin in solution binds with the immobilized biotin on the nanofiber surface when the membrane is added to the solution

Confocal microscopy was used to image the fluorescent emission of the bound streptavidin-FITC, shown in Table 4.4.

Table 4.4: Fluorescence microscopy results of streptavidin-FITC binding to biotin-cellulose nanofiber membranes

		Click Reaction Components				Confocal Fluorescent Microscopy
Role		Click Molecule		Catalyst		
Chemical		Alkyne-RC	Azide-Biotin	$CuSO_4$	Ascorbic Acid	
Reaction		X	X	X	X	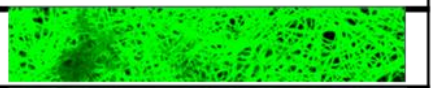
Control	1		X	X	X	
	2		X	X		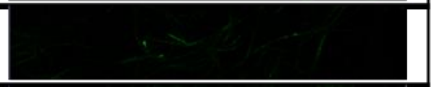
	3	X		X	X	
	4	X	X		X	
	5	X	X	X		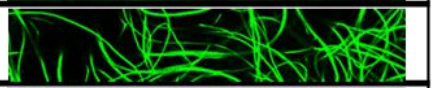
	6	X	X			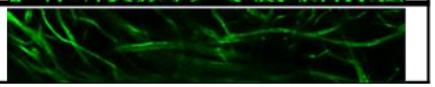

The lack of fluorescence of Control 3 confirms that no nonspecific binding of the streptavidin-FITC is occurring. Control 1 and 2 show that the alkyne moiety is required for the biotin conjugate to be immobilized and bind with the streptavidin-FITC. This suggests that the biotin conjugate is successfully clicking with the alkyne-RC and not just physically being absorbed onto the fibers. Control 5 contains copper sulfate but not ascorbic acid to reduce it to its catalyst oxidation state. Control 6 contains no catalyst and can only react at uncatalyzed amounts. Therefore, both Control 5 and 6 have less intense fluorescence than the full reaction sample due to smaller yield. The yield will be quantified in the next section.

4.3.3. Biotin Quantification

The click reaction yield was quantified using HABA Colorimetric Assay and XPS. Figure 4.17 describes the assay process for the biotin-cellulose nanofiber membrane samples.

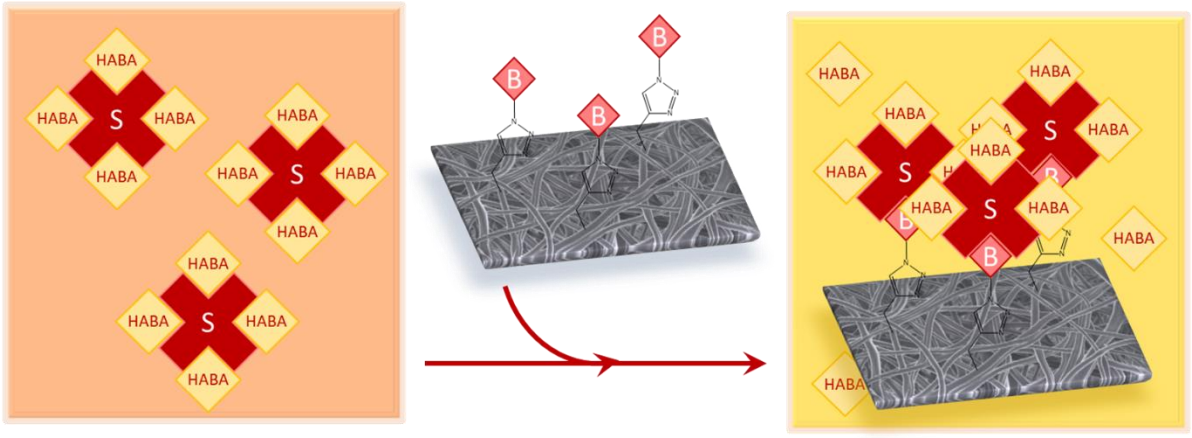

Figure 4.17: HABA Colorimetric Assay schematic: Streptavidin forms a complex with HABA molecules initially, but once biotinylated membrane is added to the mixture, the streptavidin will favorably bind with the available biotin. The change in absorbance at 500 nm correlates to the surface available biotin.

Equation 3.4 was used to calculate the degree of substitution of the biotin from the HABA results. The HABA Colorimetric Assay was performed on the biotin-cellulose samples at 1.5, 3.5, and 5 months of ageing in a desiccator, shown in Figure 4.18.

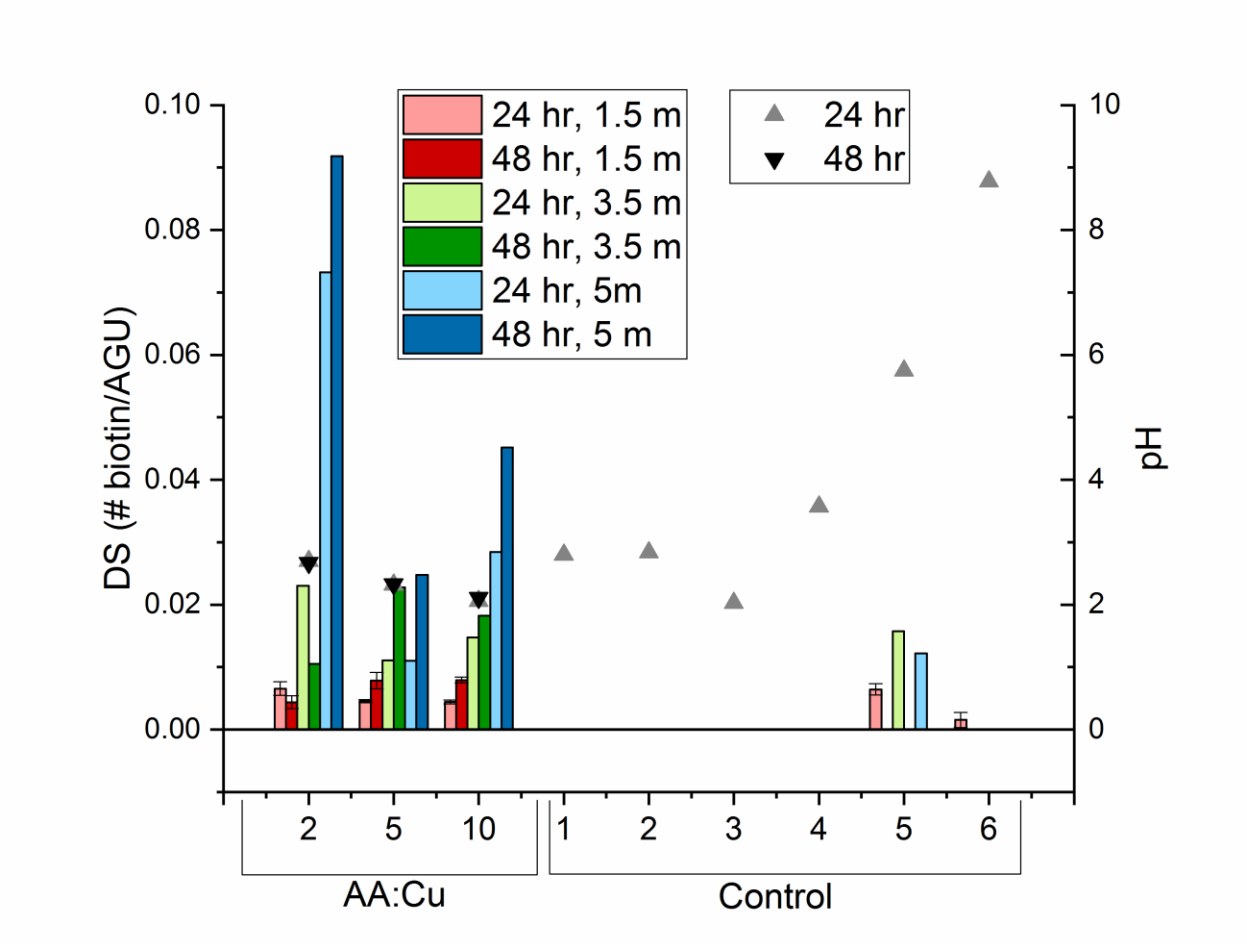

Figure 4.18: Degree of substitution of biotin on cellulose nanofibers calculated from HABA Colorimetric Assay increases with ageing over a period of 5 months

The 1.5-month samples were measured on four separate pieces of the original mat. The 3.5- and 5-month samples were only measured on one piece of original mat. Controls 1-4 had pieces of the mats detach and float in the solution, causing the absorbance values to increase (resulting in negative calculated biotin values). Even after letting the solution sit for an hour, the pieces only partially settled down. Therefore, controls 1-4

show no detected biotin in Figure 4.16. One mat for Control 6 also had this problem, which accounts for the standard deviation bars reaching below zero.

For the 1.5-month samples, the HABA assay shows that the biotin yield increases with both increase in reaction time and ascorbic acid to copper sulfate ratio. The excess ascorbic acid ensures that enough Cu(II) is reduced to Cu(I) so as to not be the limiting step in the reaction. The ascorbic acid also lowers the pH of the solution, which is below the isoelectric point of the biotin (5.1). The protonated biotin causes it to contract and not be able to participate in the reaction as much. It can also denature proteins when the project gets to that point. Control 5 does not contain ascorbic acid and has a pH above biotin's pI. This sample's yield was higher than any of the trials with both components of the catalyst. The copper (I) was proven to be generated via alcohol oxidation and terminal alkyne homocoupling.[32] Removing the need for a reducing agent is important for bioconjugation applications such as protein and antibody immobilization. Ascorbic acid reduces the pH into the range that can disturb the structure of the biomolecule, and the reduced form of ascorbic acid, dehydroascorbate, can react with certain amino acids that change the protein functionality and/or cause protein aggregation.[32] Control 6 has no ascorbic acid or copper sulfate, so only a negligible amount of uncatalyzed click reaction is occurring. Control 6 further supports the assertion that Control 5 is being catalyzed via an alternative route.

All click reaction samples were stored in a desiccator for 5 months and were retested at the 3.5- and 5-month marks. Overall, surface available biotin increased exponentially with storage time for all full reaction samples. Control 5 increased between 1.5 and 3.5 months but decreased for 5-months. Since only one piece of the membrane was tested

for each 3.5- and 5-month sample, more samples would need to be tested to determine a more robust trend between full catalyst and half catalyst (no ascorbic acid). Both alkyne and biotin have lower surface energy than cellulose, so they should stay on the surface and not migrate to inside the fiber. Since the click reaction is carried out in aqueous solution, the water molecules break the interchain hydrogen bonds that allow for the chains to reorient themselves during the reaction and the hydrogen bonds to reform in the new configuration while drying. The biotin molecules that were not available to bind with the streptavidin during the initial HABA assays will resurface over time due to the difference in surface energies that forces the biotin to the surface to minimize surface energy. The reverse phenomenon was observed when samples after 5 months of storage were re-submerged in water for 24 hours and 7 days. Both submersion times resulted in complete disappearance of the surface available biotin in the HABA assays. Normalized FTIR spectra of the samples before and after water submersion showed that the characteristic biotin peaks had no change in absorbance. This supports the hypothesis that the biotin does not leach away from the fibers when submerged in water, but instead rotates below the surface of the fibers due to the water molecules favorably hydrogen bonding with the cellulose hydroxyl groups. An exploratory experiment with heat treatment suggests that low temperature (40°C – 80° C) application can drive the biotin to resurface. A more in-depth study is required to determine how controllable the surface biotin availability is. For the diagnostic device application, short contact times (up to one hour) seem to not affect the surface composition of the cellulose nanofibers.

The degree of substitution of the biotin after 5 months was also calculated from the XPS results using Equation 3.2. The ratio of sulfur to carbon was calculated from the XPS survey scans. Figure 4.19 shows the comparison of the degree of substitution of biotin calculated from HABA and XPS.

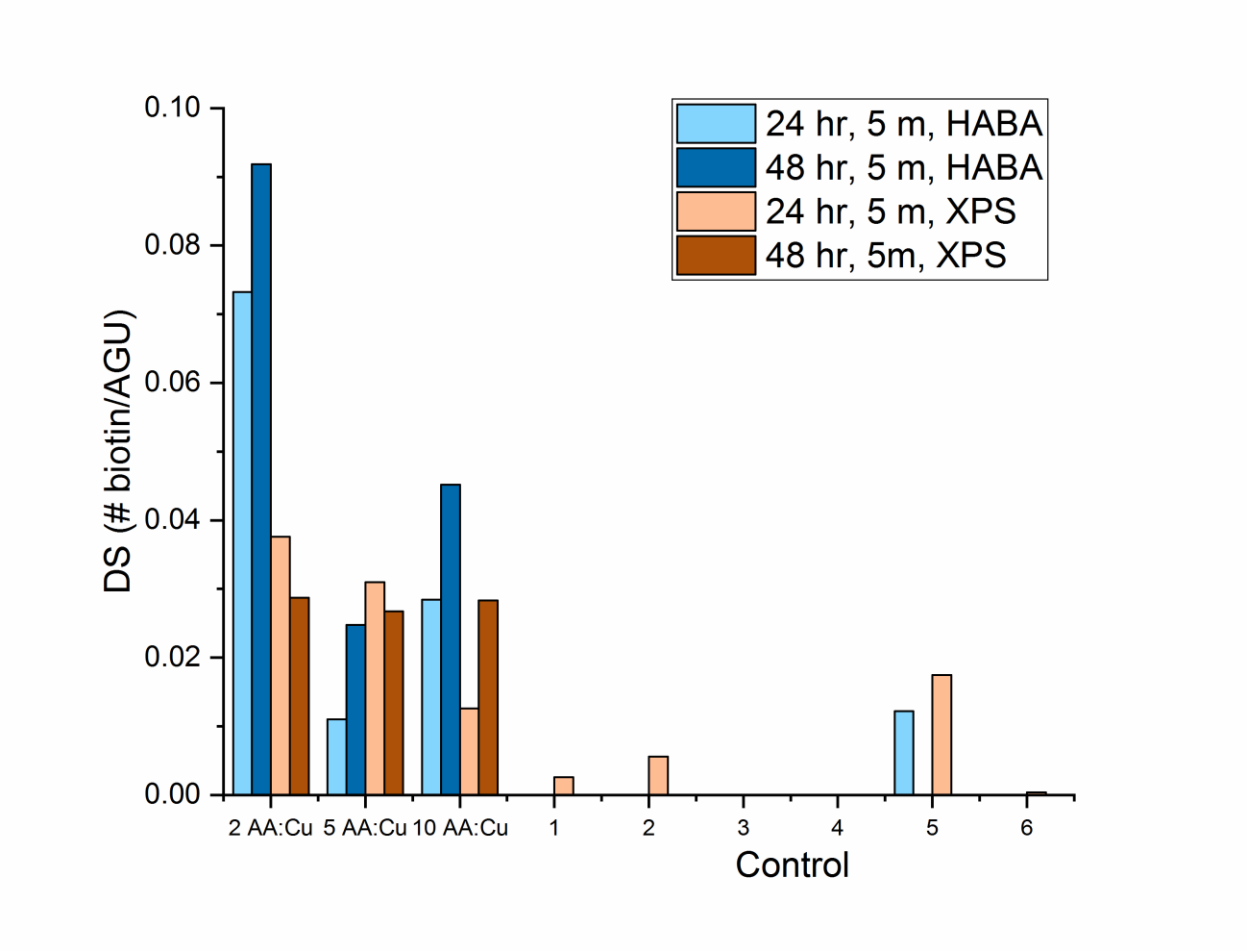

Figure 4.19: Degree of substitution of biotin on cellulose nanofibers after 5 months of storage calculated from HABA Colorimetric Assay and XPS survey scans

HABA quantifies only the amount of biotin available to bind with the streptavidin in solution. The HABA assay will not account for any diffusion limitations as well as any biotin that has been chemically modified or resides in a conformation that makes it unavailable to bind with streptavidin. XPS detects all carbon and sulfur present on the

sample. Therefore, it can detect total surface biotin regardless of configuration or chemical modification. Two main disadvantages to XPS for cellulose nanofibers are carbon contamination that can accumulate on the surface of the samples as well as the shadowing effect of the round nanofibers. Both sources of error can reduce the sulfur to carbon ratio and result in lower DS results as seen in the 2 AA:Cu ratio samples. Overall, the XPS and HABA DS calculations are mostly in agreement.

5. CONCLUSIONS

Cellulose nanofiber membranes were successfully functionalized with biotin conjugate via click chemistry. The intermediate step of alkyne substitution onto cellulose was dependent on ratio of solvents, time, and temperature. CA required a water-rich solvent system whereas RC had higher FTIR peak height ratios in an isopropanol-rich solvent system. The alkyne nucleophilic substitution reaction competed with byproduct reactions, and therefore, the alkyne substitution onto cellulose was optimized with reaction conditions that minimized the reaction rates of these competing reactions. Both alkyne substitution methods only modified the surface of the nanofibers and did not disturb the bulk. The two-step (RC) compared to the one-step (CA) alkyne substitution method achieved a higher alkyne yield at 80% lower NaOH concentration, less membrane degradation, and 6 times faster reaction (2 hours deacetylation plus 6 hours alkyne substitution compared to 48 hours alkyne substitution). The two-step method uses milder reaction conditions and is still more efficient than the one-step method, so only the two-step method was used for the click reaction experiments.

The CuAAC click reaction step revealed two major findings:

1. With all click reaction components, the initial apparent biotin yield is dependent on ratio of ascorbic acid to copper sulfate, pH, and time.
2. Click reaction controls confirmed the selectivity and specificity of the reaction; catalysis is possible without a reducing agent as seen with Control 5.

Ascorbic acid acts as the reducing agent for copper (II) to copper (I) as well as lowers the pH of the reaction solution. Biomolecules such as proteins will unfold, or their amino residues will react in acidic pH, causing them to lose their bioactivity. Loss of bioactivity must be avoided, and therefore, performing the click reaction without a reducing agent is desirable. Control 5 was free of ascorbic acid and proven to successfully click the biotin conjugate onto the cellulose nanofibers' surface. Further, the surface available biotin of Control 5 was stable with storage over a period of 5 months. The surface available biotin for the samples with both copper sulfate and ascorbic acid increased with storage. The proposed mechanism of ageing is based on the cellulose chain mobility and the minimization of free surface energy. During the reaction, the water molecules disrupt the intra- and intermolecular hydrogen bonding of the cellulose chains, causing the cellulose fibers to swell in the aqueous solution. The azide-biotin conjugate forms triazole rings with the available alkynes. Once the cellulose membrane is removed from the aqueous solution, the hydroxyl groups remain in their conformation, which causes some biotin to not be available to bind with the streptavidin in the HABA colorimetric assay. Over time, the cellulose chains can rotate the lower energy biotin to the surface to minimize the free surface energy. Therefore, the surface chemistry of the cellulose nanofibers can be controlled by immersing the membrane in water to force the biotin below the surface and storing the membrane in air to allow the biotin to resurface.

The degree of substitution of biotin was calculated to be between 0.01 and 0.10 from both the HABA colorimetric assay and XPS. This magnitude of DS translates to one biotin molecule per every 10 to 100 AGU. The repeat unit of cellulose, cellobiose, contains two AGU and has a unit length of approximately 1.03 nm.[33] Therefore, the biotin is on average spaced 5 to 50 nm apart from each other. This biotin spacing is useful for filtration and diagnostic device applications as it allows for target and amplification molecules' immobilization onto the pendant biotin. For example, streptavidin is approximately 5 nm and fits well within the biotin spacing.[34] Amplification molecules rely on proper spacing of the first layer (ie. biotin) so that subsequent molecules can bind without steric hindrance in sandwich assays.

6. RECOMMENDATIONS FOR FUTURE STUDIES

While reducing agent-free CuAAC click reaction was achieved in this work, a variety of other options can be explored for increasing the yield of biologically friendly click reactions onto nanofiber membranes. These include ligand-assisted, alternative sources of copper (I), and strain-promoted (SPAAC). Cellulose was used in this work to attach alkyne to the fiber and click an azide conjugate, but other fiber-forming polymers can be used for their nitrogen content such as chitosan, wool, and nylon. The nitrogen groups could be transformed into azide groups and used to form triazole rings with alkyne conjugates. Polyacrylonitrile has the potential to be used without the initial azide modification step and form a tetrazole ring originating from the nitrile group. These alternative fibers would need to be studied individually based on their nitrogen group availability and reactivity.

The next step with the biotin-cellulose nanofiber membranes are to further explore the controlled surface availability of biotin. The biotin can reversibly disappear from the surface by immersing the nanofiber membranes in water for 24 hours, but the resurfacing requires a much longer time, on the scale of months, in ambient air. Building upon the exploratory experiments conducted, heat treatment could potentially accelerate the chain mobility to reliably control the resurfacing of the biotin in a shorter time period. A Design of Experiments with temperature, relative humidity, and time would locate the optimal conditions. The controllable surface chemistry could have larger implications in other applications such as controlled drug release, temperature or moisture responsive fabrics, etc.

For next steps in the diagnostic device design, the biotin-cellulose nanofibers will be incorporated into microfluidic channels for dynamic testing of selective capture of streptavidin. The biotin-streptavidin model can also be replaced with an antibody-antigen model where the antibody is directly clicked onto the nanofiber surface and used to detect the antigen in the sample fluid. Sandwich assays and multiplexing of multiple target molecules will be designed and tested using the clicked nanofiber membranes.

7. REFERENCES

[1] World Health Organization. (2016). World Health Statistics 2016: Monitoring Health for the SDGs, Sustainable Development Goals. Geneva. E-ISBN 978 92 4 069569 6 (PDF)

[2] Rebelo, R., Barbosa, A. I., Caballero, D., Kwon, I. K., Oliveira, J. M., Kundu, S. C., Reis, R. L., & Correlo, V. M. (2019). 3D biosensors in advanced medical diagnostics of high mortality diseases. Biosensors and Bioelectronics, 130, 20–39. https://doi.org/10.1016/j.bios.2018.12.057

[3] Mahmoudifard, M., Vossoughi, M., Soudi, S., & Soleimani, M. (2018). Electrospun polyethersolfone nanofibrous membrane as novel platform for protein immobilization in microfluidic systems. Journal of Biomedical Materials Research Part B: Applied Biomaterials, 106(3), 1108–1120. https://doi.org/10.1002/jbm.b.33923

[4] Rodriguez-deLuna, S. E., Moreno-Cortez, I. E., Garza-Navarro, M. A., Lucio-Porto, R., Lopez Pavon, L., & Gonzalez-Gonzalez, V. A. (2017). Thermal stability of the immobilization process of horseradish peroxidase in electrospun polymeric nanofibers. Journal of Applied Polymer Science, 134(19), 44811 (10 pp.). https://doi.org/10.1002/app.44811

[5] Afshari, E., Mazinani, S., Ranaei-Siadat, S.-O., & Ghomi, H. (2016). Surface modification of polyvinyl alcohol/malonic acid nanofibers by gaseous dielectric barrier discharge plasma for glucose oxidase immobilization. Applied Surface Science, 385, 349–355. https://doi.org/10.1016/j.apsusc.2016.05.119

[6] Shepherd, L. M., Gonzalez, E., Chen, E. X., & Frey, M. W. (2017). Increasing Stability of Biotin Functionalized Electrospun Fibers for Biosensor Applications. Acs Applied Materials & Interfaces, 9(2), 1968–1974. https://doi.org/10.1021/acsami.6b14348

[7] Ramakrishna, S. (2005). An introduction to electrospinning and nanofibers. Singapore: World Scientific.

[8] Sagitha, P., Reshmi, C. R., Sundaran, S. P., & Sujith, A. (2018). Recent advances in post-modification strategies of polymeric electrospun membranes. European Polymer Journal, 105, 227–249. https://doi.org/10.1016/j.eurpolymj.2018.05.033

[9] Tungprapa, S., Puangparn, T., Weerasombut, M., Jangchud, I., Fakum, P., Semongkhol, S., Meechaisue, C., & Supaphol, P. (2007). Electrospun cellulose acetate fibers: Effect of solvent system on morphology and fiber diameter. Nanotechnology: A Fiber Perspective, 14(6), 563–575. https://doi.org/10.1007/s10570-007-9113-4

[10] Fei, P., Liao, L., Cheng, B., & Song, J. (2017). Quantitative analysis of cellulose acetate with a high degree of substitution by FTIR and its application. Analytical Methods, 9(43), 6194–6201. https://doi.org/10.1039/C7AY02165H

[11] Frey, M. W. (2008). Electrospinning Cellulose and Cellulose Derivatives. Polymer Reviews, 48(2), 378–391. https://doi.org/10.1080/15583720802022281

[12] Liu, H., & Hsieh, Y.-L. (2002). Ultrafine fibrous cellulose membranes from electrospinning of cellulose acetate. Journal of Polymer Science, Part B: Polymer Physics, 40(18), 2119–2129. https://doi.org/10.1002/polb.10261

[13] Ghorani, B., Russell, S. J., & Goswami, P. (2013). Controlled Morphology and Mechanical Characterisation of Electrospun Cellulose Acetate Fibre Webs. International Journal of Polymer Science, 256161 (12 pp.). https://doi.org/10.1155/2013/256161

[14] De Vrieze, S., Van Camp, T., Nelvig, A., Hagström, B., Westbroek, P., & De Clerck, K. (2009). The effect of temperature and humidity on electrospinning. Journal of Materials Science, 44(5), 1357–1362. https://doi.org/10.1007/s10853-008-3010-6

[15] C. Hansen, Hansen Solubility Parameters: A User's Handbook, CRC Press, Boca Raton, Fla, USA, 1st edition, 2000.

[16] Hansen, C. M., The Three Dimensional Solubility Parameter and Solvent Diffusion Coefficient, Doctoral Dissertation, Danish Technical Press, Copenhagen, 1967.

[17] Chan, L., Cross, H. F., She, J. K., Cavalli, G., Martins, H. F. P., & Neylon, C. (2007). Covalent Attachment of Proteins to Solid Supports and Surfaces via Sortase-Mediated Ligation. PLoS ONE, 2(11). https://doi.org/10.1371/journal.pone.0001164

[18] Li, L., & Zhang, Z. (2016). Development and Applications of the Copper-Catalyzed Azide-Alkyne Cycloaddition (CuAAC) as a Bioorthogonal Reaction. Molecules, 21(10). https://doi.org/10.3390/molecules21101393

[19] Lu, T., Chen, X., Shi, Q., Wang, Y., Zhang, P., & Jing, X. (2008). The immobilization of proteins on biodegradable fibers via biotin-streptavidin bridges. Acta Biomaterialia, 4(6), 1770–1777. https://doi.org/10.1016/j.actbio.2008.05.006

[20] Shi, Q., Chen, X., Lu, T., & Jing, X. (2008). The immobilization of proteins on biodegradable polymer fibers via click chemistry. Biomaterials, 29(8), 1118–1126. https://doi.org/10.1016/j.biomaterials.2007.11.008

[21] Lahann, J. (Ed.). (2009). Click Chemistry for Biotechnology and Materials Science. John Wiley & Sons, Ltd.

[22] Bock, V. D., Hiemstra, H., & Maarseveen, J. H. van. (2006). CuI-Catalyzed Alkyne–Azide “Click” Cycloadditions from a Mechanistic and Synthetic Perspective. European Journal of Organic Chemistry, 2006(1), 51–68. https://doi.org/10.1002/ejoc.200500483

[23] Worrell, B. T., Malik, J. A., & Fokin, V. V. (2013). Direct Evidence of a Dinuclear Copper Intermediate in Cu(I)-Catalyzed Azide-Alkyne Cycloadditions. Science, 340(6131), 457–460. https://doi.org/10.1126/science.1229506

[24] Celebioglu, A., Demirci, S., & Uyar, T. (2014). Cyclodextrin-grafted electrospun cellulose acetate nanofibers via Click reaction for removal of phenanthrene. Applied Surface Science, 305, 581–588. https://doi.org/10.1016/j.apsusc.2014.03.138

[25] Mangiante, G., Alcouffe, P., Burdin, B., Gaborieau, M., Zeno, E., Petit-Conil, M., Bernard, J., Charlot, A., & Fleury, E. (2013). Green Nondegrading Approach to Alkyne-Functionalized Cellulose Fibers and Biohybrids Thereof: Synthesis and Mapping of the Derivatization. Biomacromolecules, 14(1), 254–263. https://doi.org/10.1021/bm3016829

[26] Webster, R., Didier, E., Harris, P., Siegel, N., Stadler, J., Tilbury, L., & Smith, D. (2007). PEGylated Proteins: Evaluation of Their Safety in the Absence of Definitive Metabolism Studies. Drug Metabolism and Disposition, 35(1), 9–16. https://doi.org/10.1124/dmd.106.012419

[27] Jevševar, S., Kunstelj, M., & Porekar, V. G. (2010). PEGylation of therapeutic proteins. Biotechnology Journal, 5(1), 113–128. https://doi.org/10.1002/biot.200900218

[28] Nelson, M. L., & O'Connor, R. T. (1964). Relation of certain infrared bands to cellulose crystallinity and crystal lattice type. Part II. A new infrared ratio for estimation of crystallinity in celluloses I and II. Journal of Applied Polymer Science, 8(3), 1325–1341. https://doi.org/10.1002/app.1964.070080323

[29] Ahvenainen, P., Kontro, I., & Svedström, K. (2016). Comparison of sample crystallinity determination methods by X-ray diffraction for challenging cellulose I materials. Cellulose, 23(2), 1073–1086. https://doi.org/10.1007/s10570-016-0881-6

[30] Knill, C. J., & Kennedy, J. F. (2003). Degradation of cellulose under alkaline conditions. Carbohydrate Polymers, 51(3), 281–300. https://doi.org/10.1016/S0144-8617(02)00183-2

[31] Yokota, H. (1985). The mechanism of cellulose alkalization in the isopropyl alcohol–water–sodium hydroxide–cellulose system. Journal of Applied Polymer Science, 30(1), 263–277. https://doi.org/10.1002/app.1985.070300121

[32] Brotherton, W. S., Michaels, H. A., Simmons, J. T., Clark, R. J., Dalal, N. S., & Zhu, L. (2009). Apparent Copper(II)-Accelerated Azide−Alkyne Cycloaddition. Organic Letters, 11(21), 4954–4957. https://doi.org/10.1021/ol9021113

[33] Thygesen, A., Oddershede, J., Lilholt, H., Thomsen, A. B., & Ståhl, K. (2005). On the determination of crystallinity and cellulose content in plant fibres. Cellulose, 12(6), 563–576. https://doi.org/10.1007/s10570-005-9001-8

[34] Avvakumova, S., Colombo, M., Galbiati, E., Mazzucchelli, S., Rotem, R., & Prosperi, D. (2018). Bioengineered Approaches for Site Orientation of Peptide-Based Ligands of Nanomaterials. In Biomedical Applications of Functionalized Nanomaterials (pp. 139–169). Elsevier. https://doi.org/10.1016/B978-0-323-50878-0.00006-9

APPENDIX

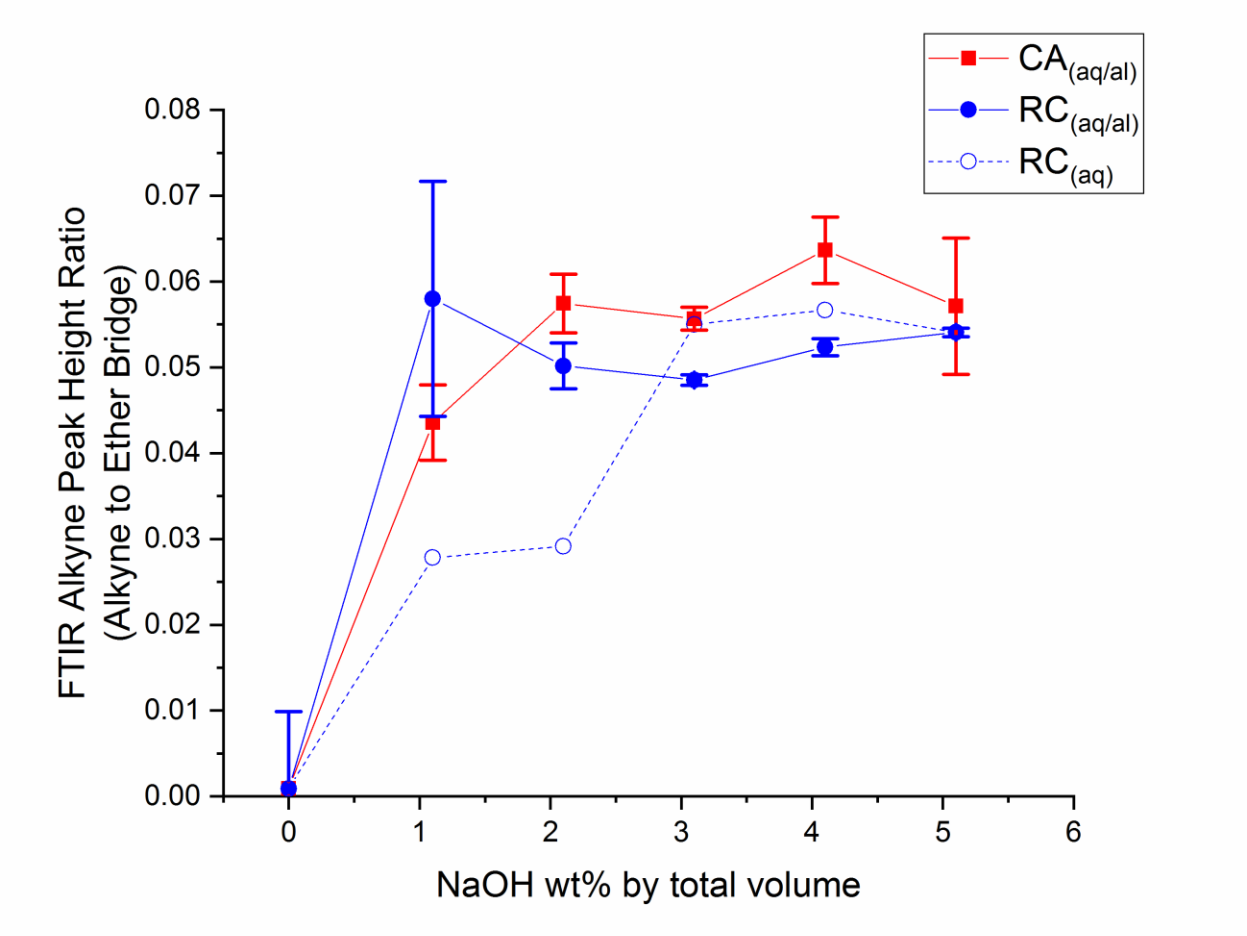

Figure A1: FTIR peak height ratios of alkyne to ether bridge for the alkyne substitution onto CA and RC in aqueous and hydroalcoholic NaOH solutions.

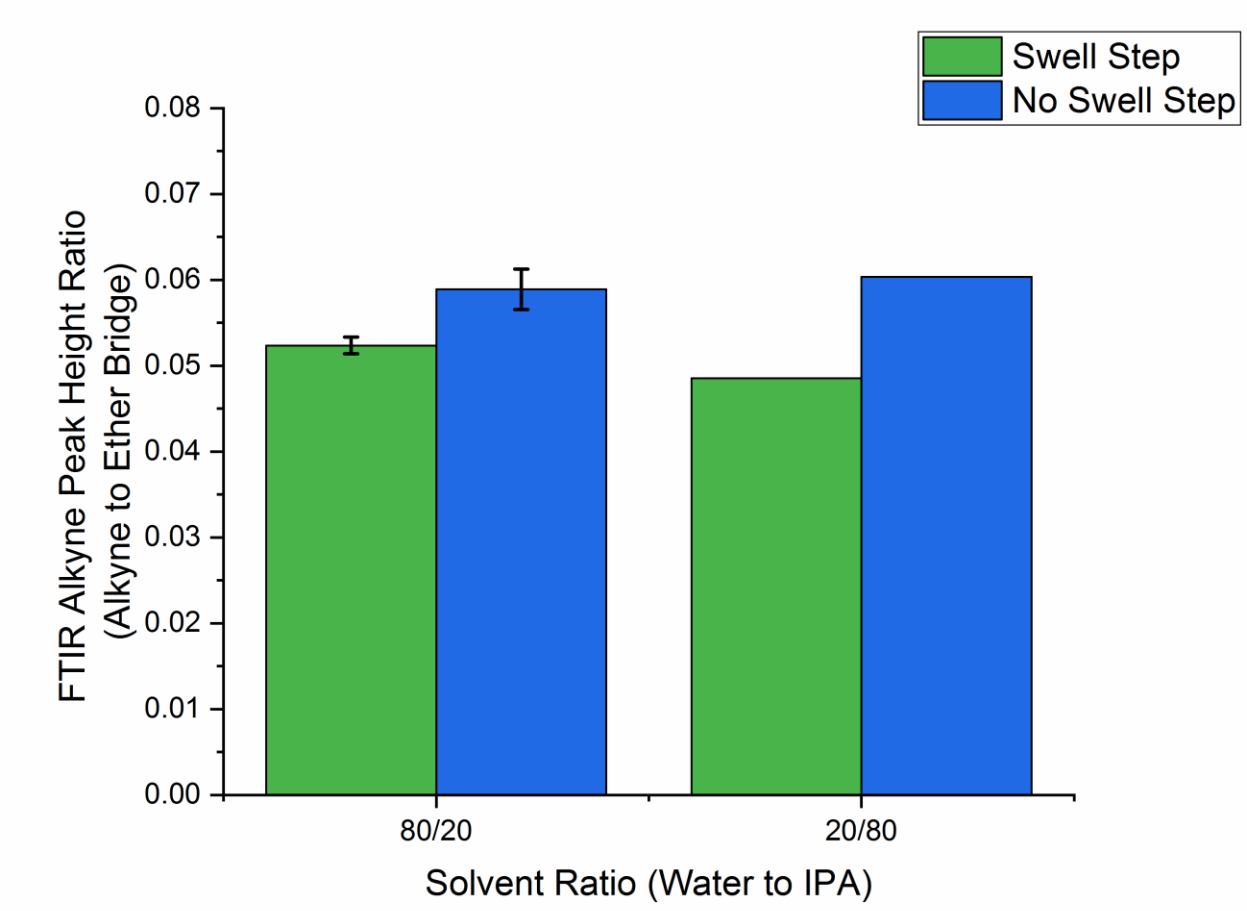

Figure A2: FTIR alkyne substitution for RC in 5.1wt% NaOH solution of 80/20 and 20/80 IPA to water with and without the fiber swell step. Omitting the swell step results in higher alkyne substitution.